Deep-Sea Research II 105 (2014) 1–16

Contents lists available at ScienceDirect

Deep-Sea Research II

journal homepage: www.elsevier.com/locate/dsr2

Phytoplankton blooms beneath the sea ice in the Chukchi sea

Kevin R. Arrigo [a,*,1], Donald K. Perovich [b,c], Robert S. Pickart [d], Zachary W. Brown [a], Gert L. van Dijken [a], Kate E. Lowry [a], Matthew M. Mills [a], Molly A. Palmer [a], William M. Balch [e], Nicholas R. Bates [f], Claudia R. Benitez-Nelson [g], Emily Brownlee [h], Karen E. Frey [i], Samuel R. Laney [h], Jeremy Mathis [j], Atsushi Matsuoka [k,l], B. Greg Mitchell [m], G.W.K. Moore [n], Rick A. Reynolds [m], Heidi M. Sosik [h], James H. Swift [m]

[a] Department of Environmental Earth System Science, Stanford University, Stanford, CA 94305, USA
[b] Engineer Research and Development Center, Cold Regions Research and Engineering Laboratory, Hanover, NH 03755, USA
[c] Thayer School of Engineering, Dartmouth College, Hanover, NH 03755, USA
[d] Department of Physical Oceanography, Woods Hole Oceanographic Institution, Woods Hole, MA 02543, USA
[e] Bigelow Laboratory for Ocean Sciences, West Boothbay Harbor, ME 04575, USA
[f] Bermuda Institute of Ocean Sciences, Ferry Reach GE01, Bermuda
[g] Marine Science Program,and Department of Earth and Ocean Sciences, University of South Carolina, Columbia, SC 29208, USA
[h] Biology Department, Woods Hole Oceanographic Institution, Woods Hole, MA 02543, USA
[i] Graduate School of Geography, Clark University, Worcester, MA 01610, USA
[j] NOAA Pacific Marine Environmental Laboratory, Seattle, WA 98115, USA
[k] Université Pierre et Marie Curie, Laboratoire d'Océanographie de Villefranche, Villefranche-sur-Mer 06238, France
[l] Takuvik Joint International Laboratory, Département de Biologie and Québec-Océan, Université Laval, Canada
[m] Scripps Institution of Oceanography, University of California San Diego, La Jolla, CA 92093, USA
[n] Department of Physics, University of Toronto, Toronto, Ontario, Canada M5S 1A7

ARTICLE INFO

Available online 3 April 2014

Keywords:
Arctic
Sea ice
Phytoplankton

ABSTRACT

In the Arctic Ocean, phytoplankton blooms on continental shelves are often limited by light availability, and are therefore thought to be restricted to waters free of sea ice. During July 2011 in the Chukchi Sea, a large phytoplankton bloom was observed beneath fully consolidated pack ice and extended from the ice edge to >100 km into the pack. The bloom was composed primarily of diatoms, with biomass reaching 1291 mg chlorophyll *a* m^{-2} and rates of carbon fixation as high as 3.7 g C m^{-2} d^{-1}. Although the sea ice where the bloom was observed was near 100% concentration and 0.8–1.2 m thick, 30–40% of its surface was covered by melt ponds that transmitted 4-fold more light than adjacent areas of bare ice, providing sufficient light for phytoplankton to bloom. Phytoplankton growth rates associated with the under-ice bloom averaged 0.9 d^{-1} and were as high as 1.6 d^{-1}. We argue that a thinning sea ice cover with more numerous melt ponds over the past decade has enhanced light penetration through the sea ice into the upper water column, favoring the development of these blooms. These observations, coupled with additional biogeochemical evidence, suggest that phytoplankton blooms are currently widespread on nutrient-rich Arctic continental shelves and that satellite-based estimates of annual primary production in waters where under-ice blooms develop are ~10-fold too low. These massive phytoplankton blooms represent a marked shift in our understanding of Arctic marine ecosystems.

1. Introduction

Over the last several decades, the Arctic Ocean has undergone unprecedented changes in sea ice, with summer minimum ice extent declining >40% since 1979 (Comiso et al., 2008) and first-year ice largely replacing the once prevalent multi-year pack ice (Maslanik et al., 2011; Nghiem et al., 2007). This has produced an ice cover that is substantially thinner and more prone to melting and transport, leading to a markedly extended period of open water, particularly over the last decade (Arrigo and van Dijken, 2011).

Associated with the loss in sea ice on these shelves has been an increase in the amount of light penetrating the surface ocean and a dramatic rise in the productivity of phytoplankton (Arrigo and van Dijken, 2011), the organisms responsible for the bulk of Arctic Ocean primary production and constitute the base of the marine food web. This is particularly true for the Pacific sector of the

* Corresponding author.
E-mail address: arrigo@stanford.edu (K.R. Arrigo).
[1] Department of Environmental Earth System Science, 473 Via Ortega, Stanford University, Stanford, CA 94305-4216, USA.

http://dx.doi.org/10.1016/j.dsr2.2014.03.018
0967-0645/

Arctic Ocean where annual production increased by 130% in the East Siberian Sea and 48% in the Chukchi Sea between 1997 and 2009 (Arrigo and van Dijken, 2011). Because sea ice and snow strongly reflect and attenuate incident solar radiation (Perovich, 1998; Perovich and Polashenski, 2012), the growth of phytoplankton at high latitudes is generally thought to begin in the open waters of the marginal ice zone (MIZ) once sea ice retreats in spring, as solar elevation increases and surface waters become stratified by the addition of sea ice melt water (Alexander and Niebauer, 1981; Loeng et al., 2005; Sakshaug, 1997; Hill and Cota, 2005; Perrette et al., 2011). In fact, all current large-scale estimates of primary production in the Arctic Ocean assume that phytoplankton production in the water column under sea ice is negligible (Subba Rao and Platt, 1984; Sakshaug, 2003; Pabi et al., 2008; Arrigo and van Dijken, 2011). However, an intense phytoplankton bloom was recently observed in the Chukchi Sea growing beneath fully consolidated sea ice ranging in thickness from 0.8 to 1.3 m (Arrigo et al., 2012). The development of this bloom has been attributed to increased light transmission through sea ice (Frey et al., 2011) as well as high nutrient concentrations on the Chukchi shelf.

The Chukchi Sea is an inflow shelf (Carmack and Wassmann, 2006) that ventilates the upper halocline of the Arctic Ocean (Woodgate et al., 2005). Water flows northward through the Bering Strait due to the sea surface height differential that results from the salinity difference between the Pacific and Arctic Oceans (Coachman et al., 1975), with the volume flux increasing by 50% between 2001 and 2011 (Woodgate et al., 2012). Upon reaching the Chukchi Sea, the Pacific-origin water separates into three branches that flow around or between Herald and Hanna Shoals (Fig. 1). Although these branches are identified based on water mass properties set within the Bering Sea (Coachman et al., 1975; Overland and Roach, 1987; Weingartner et al., 2005), they also differ significantly with respect to nutrient concentrations (Walsh et al., 1989; Cooper et al., 1997; Codispoti et al., 2005, 2013). The easternmost Alaska Coastal Water (ACW) is relatively warm (1–6 °C), fresh ($S < 31.8$), and nutrient-poor ($NO_3^- < 10$ μM) due to the input of river runoff and the biological drawdown of nutrients in the eastern Bering Sea. The Central Channel pathway consists of Bering Shelf Water with moderate nutrients ($NO_3^- \sim 15$ μM) and salinity (31.8–32.5). The westernmost Herald Canyon pathway, containing mostly Anadyr Water, has the highest salinity (32.5–33) and nutrient concentrations (pre-bloom $NO_3^- > 25$ μM) due to the under-utilization of nutrients in the western Bering Sea (Hansell et al., 1993). Upon reaching the shelf break, some of this water turns eastward and flows toward the Beaufort Sea in a relatively swift shelf break jet (Weingartner et al., 2005).

Water mass properties in the Chukchi Sea are further influenced by the seasonal cycle of sea ice. In the winter, brine rejection during sea ice formation mixes the entire water column to extremely cold temperatures (−1.8 °C) (Woodgate et al., 2006). Sea ice formation in polynyas and leads continue to convectively form cold and dense winter water (WW) on the Chukchi shelf throughout the winter. A large fraction of this becomes nutrient-rich Pacific Winter Water that drains through the Chukchi Sea in the spring and eventually fills the Arctic Ocean halocline. As sea ice retreats in spring and summer, the water column becomes re-stratified as surface waters freshen and warm (Woodgate and Aagaard, 2005). WW remaining on the Chukchi shelf in the summer is gradually replaced by relatively warm Pacific Summer Water (Weingartner et al., 2005).

Because of its high nutrient content, the Chukchi Sea is a region of intense summer biological activity with a rich benthic

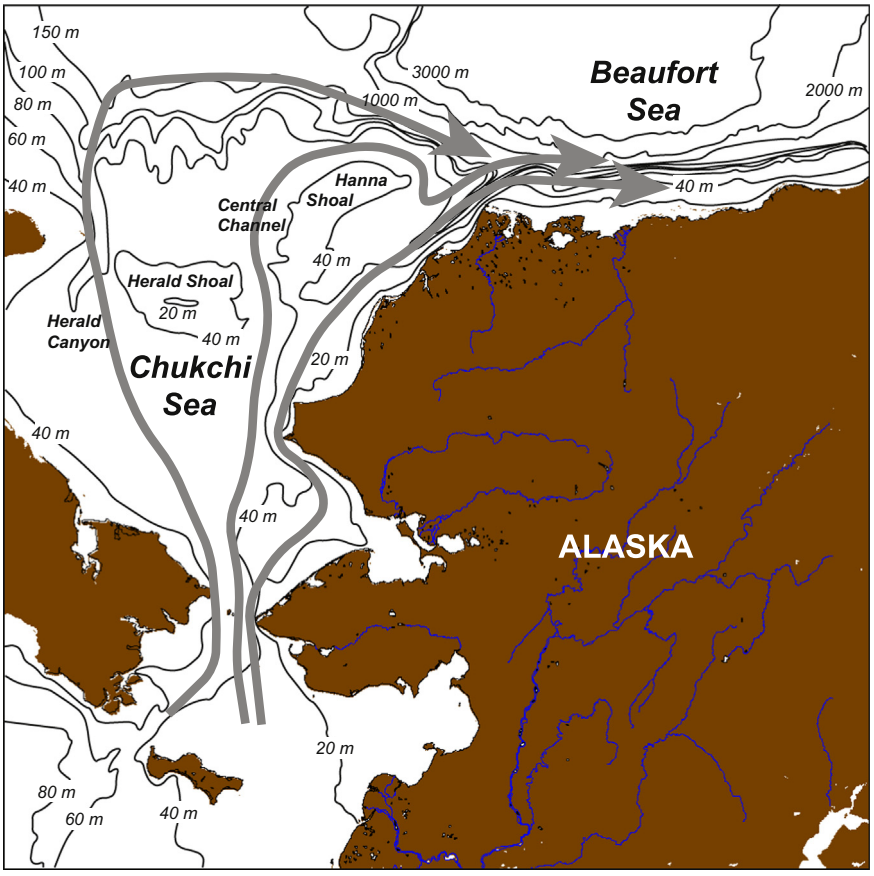

Fig. 1. Map of the Chukchi Sea showing the major bathymetric features and the predominant flow paths from the Bering Sea. Currents modified from Weingartner et al. (2005).

community that supports abundant populations of marine mammals and seabirds (Loeng et al., 2005; Dunton et al., 2005; Grebmeier et al., 2006). Depth-integrated primary production and chlorophyll *a* (Chl *a*) in the Chukchi Sea are among the highest in the world (Springer and McRoy, 1993; Arrigo et al., 2012). Phytoplankton contribute >90% of the total primary production in the Chukchi Sea (Hill and Cota, 2005), although sea ice algal production can be important early in the season (Gradinger, 2009). Intense phytoplankton blooms have been observed throughout the Chukchi shelf, with spatial variation attributed to differences in water masses, nutrient availability, and environmental forcing (Cota et al., 1996; Wang et al., 2005; Lee et al., 2007). The southeastern Chukchi Sea and Barrow Canyon have specifically been identified as hot spots for primary production (Sukhanova et al., 2009), while waters near the coast of Alaska in the ACW (Coupel et al., 2012) and off the continental slope generally have lower biomass (Lee et al., 2012).

Here we present the results from the recent ICESCAPE (Impacts of Climate on EcoSystems and Chemistry of the Arctic Pacific Environment) program documenting in greater detail the physical, chemical, and biological characteristics of an intense phytoplankton bloom observed below the first year sea ice of the Chukchi Sea (Arrigo et al., 2012). The present paper provides an overview of the observed under-ice phytoplankton bloom. Companion papers in this issue address more specific aspects of the bloom, including (1) the hydrographic conditions leading to the large accumulations of algal biomass beneath the ice (Spall et al., 2014), (2) the ice conditions required for under-ice bloom development (Palmer et al., 2014), (3) the types of phytoplankton observed in association with the bloom (Laney and Sosik, 2014), (4) the impact of the under-ice bloom on the optical properties of the water column (Neukermans et al., 2014), the response of the bacterial community to the under-ice phytoplankton bloom (Ortega-Retuerta et al., 2014), and a satellite-based analysis of the frequency of under-ice phytoplankton blooms on the Chukchi shelf in the recent past (Lowry et al., 2014). Observations made within the sea ice zone (SIZ) on the Chukchi shelf contradict the common perception that waters beneath the consolidated ice pack harbor little phytoplankton biomass. Instead, our results suggest that phytoplankton growing beneath a thinner Arctic ice pack composed mostly of first year ice can contribute greatly to annual primary production, and even exceed rates measured in open waters after the sea ice has retreated.

2. Methods

2.1. Study region

During the ICESCAPE program, we sampled the Chukchi Sea continental shelf between the Bering Strait and the western Beaufort Sea from 18 June through 16 July 2010 and from 28 June through 24 July 2011 onboard the USCGC *Healy*. We sampled 140 stations (including 10 sea ice stations) in 2010 and 172 stations (including 9 sea ice stations) in 2011. Here we focus on stations 46–57 (Transect 1) and 57–71 (Transect 2) sampled from 3–8 July 2011 (Fig. 2A) but also refer to stations 38–55 (29–30 June) and 71–84 (6–7 July) sampled in 2010 (Fig. 2C). These stations were located along four different transects that extended from open water into the pack ice and all exhibited evidence of an under-ice phytoplankton bloom (Fig. 2).

At each station, water column profiles of temperature, salinity, and oxygen were measured using a conductivity, temperature, and depth sensor (Sea-Bird Electronics) and oxygen sensor (SBE43, Sea-Bird Electronics) attached to a rosette. Mixed layer depth (MLD) was calculated as the depth where potential density exceeded the surface value by 0.05. Water was collected at standard depths (5, 10, 25, 50, 75, 100, 150, and 200 m) and at the depth of the fluorescence maximum into 30 L Niskin bottles. Current speed and direction were measured with a hull mounted Ocean Surveyor 150 KHz ADCP (Teledyne RD Instruments, OS150).

Sea ice thickness. Sea ice thickness was measured directly by drilling holes through the ice. Surveys of ice thickness were also conducted using a Geonics EM-31 electromagnetic induction sensor that determines the ice thickness with an accuracy of ± 0.05 m by exploiting the large conductivity difference between sea ice and the underlying seawater (Eicken et al., 2001). The instrument transmits a primary electromagnetic field and measures the strength of a secondary field induced in the ocean. The induced field strength is related to the distance from the instrument to the seawater and therefore the ice thickness.

2.2. Phytoplankton

Chlorophyll a. Underway seawater was pumped from a depth of 8 m as part of the Uncontaminated Science Seawater System (USSS). Some of this seawater was diverted to a WETLabs WETSTAR flow-through fluorometer. Fluorescence was converted to Chl *a* concentration by calibrating against Chl *a* concentrations measured in discrete seawater samples (see below) that were collected at least four times daily from the USSS.

Samples for fluorometric analysis of Chl *a* were filtered onto 25 mm Whatman GF/F filters (nominal pore size 0.7 μm), placed in 5 mL of 90% acetone, and extracted in the dark at 3 °C for 24 h. Chl *a* was measured fluorometrically (Holm-Hansen et al., 1965) using a Turner 10-AU (Turner Designs, Inc.). The fluorometer was calibrated using a pure Chl *a* standard (Sigma).

Particulate organic carbon. Particulate organic carbon (POC) samples were collected by filtering water samples onto precombusted (450 °C for 4 h) 25 mm Whatman GF/F filters. Filter blanks were produced by passing ~50 mL of 0.2 μm filtered seawater through a GF/F. All filters were then immediately dried at 60 °C and stored dry until analysis. Prior to analysis, samples and blanks were fumed with concentrated HCl, dried at 60 °C and packed into tin capsules (Costech Analytical Technologies, Inc.) for elemental analysis on a Elementar Vario EL Cube (Elementar Analysensysteme GmbH, Hanau, Germany) interfaced to a PDZ Europa 20–20 isotope ratio mass spectrometer (Sercon Ltd., Cheshire, UK). Standards included peach leaves and glutamic acid.

Fast repetition rate fluorometry. The maximum efficiency of photosystem II (Fv/Fm) of discrete samples was determined by fast repetition rate fluorometry (FRRf) (Kolber et al., 1998) on a custom made instrument (Z. Kolber). Samples were dark adapted for 30 min at in situ seawater temperatures before measurement with the FRRf. Blanks for individual samples analyzed by FRRf were prepared by gentle filtration through a 0.2 μm polycarbonate syringe filter before measurement using identical protocols. All reported values of Fv/Fm have been corrected for blank effects (Cullen and Davis, 2003).

Photosynthesis vs. Irradiance. P–E parameters (P^*_m – maximum photosynthetic rate, α^* – photosynthetic efficiency, and E_k – photoacclimation parameter) were determined using a modified ^{14}C-bicarbonate incorporation technique (Lewis and Smith, 1983; Arrigo et al., 2010). Carbon uptake, normalized by Chl *a* concentration, was calculated from radioisotope incorporation, and the data were fit by least squares nonlinear regression to the equation of Platt et al. (1980). *P–E* parameters were used with under-ice light profiles to estimate rates of depth-integrated daily gross primary production. Specific growth rate (μ, d^{-1}) for a given sample was calculated by multiplying the photosynthetic rate (P^*) by the Chl *a*:POC ratio from that sample.

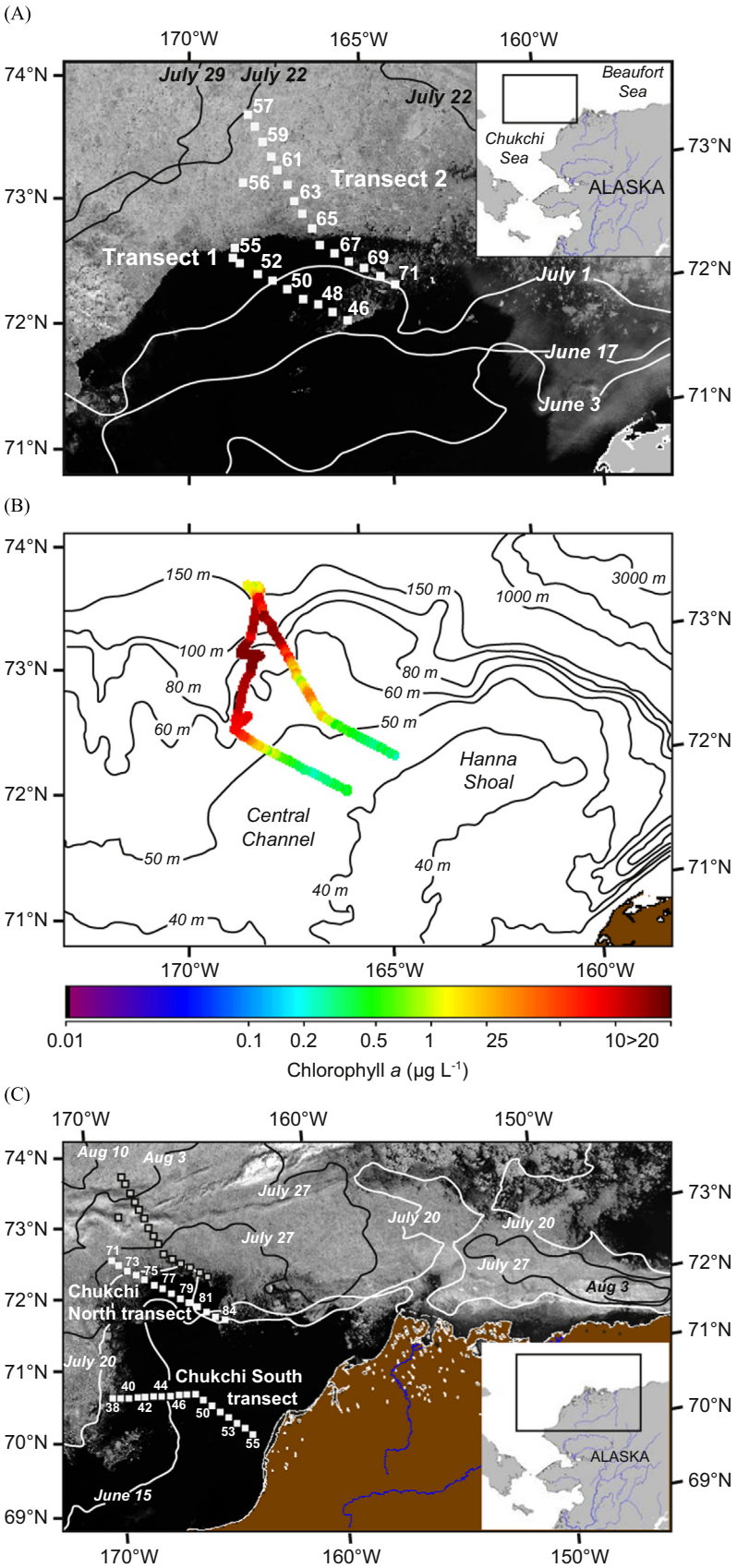

Fig. 2. Maps of the northern Chukchi Sea showing (A) the distribution of sea ice on 8 July 2011 (MODIS-Aqua) and the location of stations sampled during the ICESCAPE 2011 cruise. Black indicates open water. Lines show the position of the ice edge on the indicated dates (AMSR-E). In the text, stations 46–57 are referred to as Transect 1 and stations 57–71 are Transect 2. (B) Bathymetry of the study area overlaid by surface chlorophyll *a* concentration calculated from fluorescence measured by the continuous seawater system of the USCGC *Healy* in July 2011. (C) Map of the Chukchi Sea showing the distribution of sea ice on 8 July 2010 and the location of select stations sampled during the ICESCAPE 2010 cruise (numbered white squares). An under-ice phytoplankton bloom of similar intensity was observed along the Chukchi North transect during ICESCAPE 2010 at the same time of year (6–7 July 2010) and in the same location as Transect 1 in ICESCAPE 2011 (for reference, other stations from ICESCAPE 2011 are shown as un-numbered gray boxes). Unfortunately, the Chukchi North transect started in the sea ice and progressed southeastward toward open water during ICESCAPE 2010, without enough transit into the ice pack to sample the full extent of the under-ice bloom.

Net primary production. Simulated in situ daily net primary production (NPP) was determined by measuring ^{14}C-bicarbonate incorporation in water samples collected from different light depths and incubated at corresponding light intensities in an on-deck incubator for 24 h. We added 0.74 MBq ^{14}C-bicarbonate to 150 mL of sample in a 250 mL Falcon flask and covered the flask with 0 to 9 layers of neutral density screens to simulate light intensities of 85, 65, 25, 10, 5 and 1% of surface irradiance. After incubation, 30 mL of sample was filtered in triplicate under very low vacuum (<50 mm Hg). Filters were acidified with 0.1 mL 6 N HCl to drive off inorganic C. After 24 h of acidification, 5 mL of scintillation cocktail (Ecolume) was added and samples were counted after >3 h on a PerkinElmer Tri-Carb liquid scintillation counter. Total activity was determined on each sample by combining 50 μL of sample with 50 μL of ethanolamine, 0.5 mL of filtered seawater, and 5 mL of scintillation cocktail. Time zero controls were filtered (30 mL in triplicate) and acidified at the start of the incubation period. Specific growth rate (μ, d^{-1}) in surface waters was calculated by normalizing the NPP rate by POC concentration.

Phytoplankton community composition. The taxonomic composition of the nano- and microphytoplankton assemblage was determined using an automated imaging flow cytometric approach. Small volumes of seawater (2.5 or 5 mL) were subsampled from bottle casts and then analyzed with an Imaging FlowCytobot (Olson and Sosik, 2007). This generated large numbers of images of individual cells of length scale ~10 to >100 μm, which were then sorted manually into appropriate taxonomic classes, typically to the genus level. The biomass contributed by cells in each class at every station and depth was estimated from the cross-sectional area of cells, quantified by automated image processing (Sosik and Olson, 2007) and calibrated with a fluorescent microsphere standard of known diameter. Taxonomic composition of nano- and micro-phytoplankton were also verified onboard ship. Samples of 50–100 mL were first filtered onto 0.4 μm polycarbonate filters (Hewes and Holm-Hansen, 1983) and then viewed with a compound light microscope equipped with standard bright field, epifluorescence, or polarized illumination for imaging all cells, chlorophyll/phycoerythrin-containing phytoplankton, or calcifying plankton, respectively.

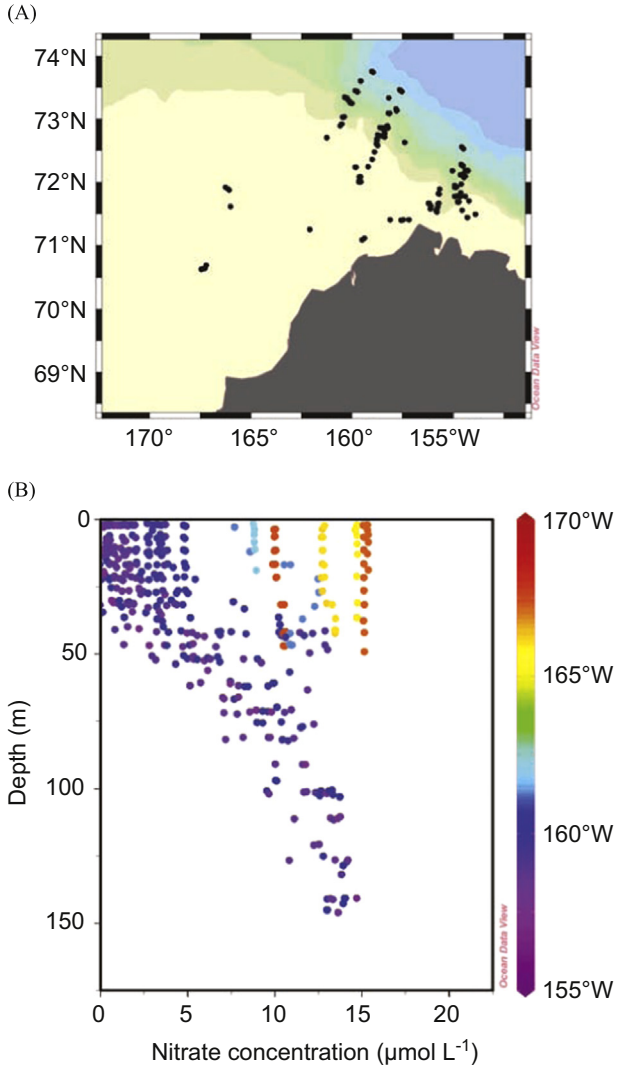

Fig. 3. Vertical nitrate profiles from the Chukchi Sea measured during the Shelf–Basin Interactions (SBI) program. (A) Map showing locations of stations sampled in May prior to significant phytoplankton growth. (B) Nitrate concentrations are high in surface waters in the western portion of the study area, reflecting convective processes on the shallow shelf that mix nutrients to the surface in winter. Colors denote longitude where samples were taken.

2.3. Nutrients, oxygen, and dissolved inorganic carbon (DIC)

Nitrate (NO_3), Oxygen, and DIC concentration. Discrete water column samples were analyzed for NO_3 and nitrite (NO_2) concentrations with a Seal Analytical continuous-flow AutoAnalyzer 3 (AA3) using a modification of the procedure by Armstrong et al. (1967). Seawater samples for DIC were drawn from the Niskin samplers into pre-cleaned ~300 mL borosilicate bottles, poisoned with $HgCl_2$ to halt biological activity, sealed, and returned to the Bermuda Institute of Ocean Sciences (BIOS) for analysis. DIC samples were analyzed using a highly precise (~0.025%; <0.5 mmoles kg^{-1}) gas extraction/coulometric detection system (Bates et al., 2005). Analyses of Certified Reference Materials (provided by A. G. Dickson, Scripps Institution of Oceanography) ensured that the accuracy of the DIC measurements was 0.05% (~0.5 mmoles kg^{-1}). The oxygen sensor on the CTD rosette (SBE43) was calibrated using standard Winkler titrations.

Nitrate and DIC deficit calculations. Water column NO_3 and DIC deficits were calculated by first assuming that the wintertime NO_3 and DIC concentrations were equal to the maximum WW concentrations measured along the study transects. WW was defined as water deeper than 10 m with a temperature below -1.65 °C. Thus, WW NO_3 and DIC concentrations over the Chukchi shelf were 24.1 and 2300 μmol L^{-1}, respectively. The value we used for WW NO_3 was virtually the same as that calculated previously (Hansell et al., 1993) for the Chukchi Shelf (23.6 ± 4.86 μmol L^{-1}). Assuming that the water column was thoroughly mixed vertically during the winter (Fig. 3), NO_3 and DIC deficits were calculated as the difference between the depth-integrated water column NO_3 or DIC during the winter and the depth-integrated water column NO_3 or DIC measured during the ICESCAPE 2011 cruise. All NO_3 and DIC concentrations were normalized to a constant salinity of 33.1 prior to making deficit calculations to correct for meltwater input.

2.4. Optics

Inherent optical properties. The beam attenuation coefficient at 488 nm was measured in situ with a C-Star transmissometer (WET Labs, Inc.) along a 25 cm path length within seawater. The spectral absorption coefficient of colored dissolved organic matter (CDOM) and particles was determined at 1 nm resolution from freshly-collected Niskin bottle samples. CDOM absorption in the sample filtrate (<0.2 μm) was measured at 200–735 nm using an UltraPath liquid waveguide system (World Precision Inc.) equipped with a 2 m pathlength. Reference water salinity was adjusted to that of the sample with pre-combusted NaCl and MilliQ water. The particle absorption coefficient (a_p) from 300 to 800 nm was

determined by collecting particles onto a 25 mm filter (Whatman GF/F) and measuring its optical density relative to a blank reference filter in a Cary 1E spectrophotometer. Spectral absorption coefficients were calculated as described in Mitchell (1990). Following measurement of a_p, sample filters were extracted in 100% methanol and re-measured to yield detrital absorption (a_d). Phytoplankton absorption (a_{ph}) was determined by difference as $a_{ph}=a_p-a_d$.

The dry mass concentration of suspended particles was determined gravimetrically on samples filtered onto pre-weighed GF/F filters, rinsed with deionized water to remove sea salt, dried at 60 °C, and measured with a Mettler-Toledo MT5 microbalance with a resolution of 0.001 mg. Particle number concentrations and size estimates were determined with a Coulter Counter Multisizer III (Beckman-Coulter) equipped with 30 μm and 200 μm aperture tubes (Reynolds et al., 2010). The estimates of particle number reported here represent the total concentration of particles over the size range of 1–100 μm. Particle median diameters were calculated from the volume distribution over this size range, and represent the diameter of a volume-equivalent sphere.

Under-ice optical measurements. Light transmittance through the ice and the upper water column was measured at stations 55, 56, and 57 (Fig. 2A). At each station, vertical light profiles were obtained beneath both representative bare ice and melt ponds. Individual sampling sites were chosen to maximize the ability to uniformly represent each ice surface type (i.e., in the center of a relatively large melt pond or in the center of a relatively large bare ice surface). An Analytical Spectral Devices Dual Detector spectroradiometer was used to measure transmitted spectral irradiance over the wavelength range of 380–850 nm. A modified Compact-Optical Profiling System (C-OPS, Biospherical Instruments Inc.) radiometer with a cosine collector was lowered to a depth of ~50 m through an auger-drilled ~25 cm hole in the ice. At the bare ice surface site, the hole was re-filled with ice tailings to mimic the previously undisturbed bare ice surface. At the melt pond site, the C-OPS was offset horizontally from the hole such that the cosine collector on the instrument looked directly up at the underside of the ice. The underwater C-OPS and surface reference sensor measured downwelling irradiance at 19 channels (320, 340, 380, 395, 412, 443, 465, 490, 510, 532, 555, 560, 625, 665, 670, 683, 710, 780 nm, and photosynthetically active radiation (PAR, 400–700 nm)). A surface reference was mounted on top of a tripod (~2.5 m above the ice surface) that stood on the ice within ~1.5 m of where the C-OPS measurements were collected.

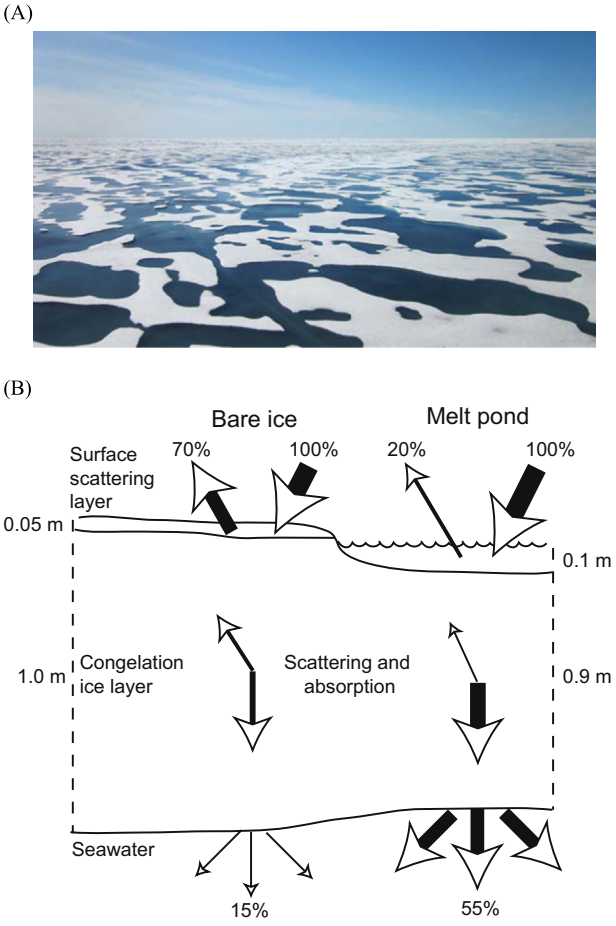

Fig. 4. Melt ponds and bare ice in the Chukchi Sea. (A) Photograph taken 13 July 2011 by Christie Wood. (B) Schematic showing light transmission through bare ice and melt ponds. Bare ice consists of a thin granular surface scattering layer that gives ice its white appearance and a thick congelation ice layer that consists of columnar ice containing numerous brine inclusions. Sea ice beneath melt ponds has no surface scattering layer and the congelation ice is generally thinner. The albedo of bare ice (70%) and melt ponds (20%) includes specular reflection at the air–ice interface and scattering of light back out of the ice interior. Light not backscattered or absorbed within the congelation ice layer is transmitted to the upper water column. Because light transmitted through the ice spreads in all directions, light levels below bare ice and melt ponds converge within ~10 m of the ice interface.

3. Results

3.1. Sea ice

During the 2011 campaign, the sea ice edge in the Chukchi Sea generally retreated from the southeast to the northwest (Fig. 2A). In the vicinity of our study area, sea ice was fully consolidated (~100% concentration) and largely undeformed, with a surface composed of a variable mix of bare ice and melt ponds (Fig. 4A). Occasionally, a northerly wind shift would push broken pack ice southward a short distance, thereby temporarily reducing ice concentrations. However, these events were short-lived and the ice edge near our study area was usually well-defined (Fig. 2A).

While much of the southern Chukchi Sea was ice-free in mid-June 2011, our study area was still covered by sea ice (Fig. 2A). By the time we started sampling Transect 1 (stations 46–71) on 3 July 2011, ice had retreated northwestward and the southern half of Transect 1 was in open water. Sampling along Transect 2 (Stations 57–71) ended on 8 July and by this time, a few more stations along Transect 1 were in open water, as were the six southernmost stations along Transect 2. By 22 July, our entire study region was ice-free.

The snow cover had melted completely by the time of our study and sea ice thickness increased significantly with distance from the ice edge. Near the edge at station 55 (Fig. 2A), mean ice thickness was 0.77 ± 0.09 m, including melt ponds that were 15–20% thinner than bare ice (Table 1). As we penetrated ~60 km deeper into the pack, ice thickness increased to 1.03 ± 0.15 m (at station 56). By station 57, approximately 120 km from the ice edge, ice thickness had increased to 1.21 ± 0.10 m. Surface melt pond fraction at the three sea ice stations averaged ~0.3. The melt ponds had well-defined boundaries and surfaces that were at sea level, implying that they were beyond the initial flooding stage (Polashenski, 2011).

3.2. Phytoplankton

From 4–8 July 2011, we sampled the full 40–150 m deep water column along Transects 1 and 2, both of which extended from open water to >100 km into the ice pack (Fig. 2A). At the time of sampling, the southeastern end of Transect 1 (station 46) had been

Table 1
Ice thicknesses and melt pond depths[a] at sea ice stations associated with under-ice phytoplankton bloom.

Station	All ice (m)		Bare ice (m)		Ponded ice (m)		Melt pond depth (m)	
	Mean	N	Mean	N	Mean	N	Mean	N
55	0.77 ± 0.09	113	0.81 ± 0.07	73	0.69 ± 0.06	40	0.05 ± 0.03	20
56	1.03 ± 0.15	198	1.10 ± 0.12	138	0.88 ± 0.07	60	0.11 ± 0.04	59
57	1.21 ± 0.10	333	1.26 ± 0.06	239	1.08 ± 0.05	94	0.12 ± 0.04	97

[a] Mean ± standard deviation.

ice-free for two weeks (Fig. 5A) and was characterized by chlorophyll *a* (Chl *a*) concentrations that were low (0.38 μg L^{-1}) within the 25 m upper mixed layer and increased to 2.5 μg L^{-1} toward the sea floor (Fig. 5B). Moving northwest along Transect 1 from open water toward the ice edge, a prominent subsurface Chl *a* maximum (SCM) that tracked the shoaling MLD (Fig. 5C) was increasingly apparent, with peak concentrations in the SCM rising from 5.4 μg L^{-1} at station 48 to 12.9 μg L^{-1} at station 51. The SCM and the MLD became progressively shallower with proximity to the ice edge. Total water column Chl *a* also increased toward the ice edge, from 43.6 mg m^{-2} at station 46 to 250 mg m^{-2} at station 51 (Fig. 6A).

Near station 52, we entered the SIZ, which had a well-defined ice edge coinciding with the westward limit of the warm water (Fig. 5D) being advected northward in the upper portion of the shelf break jet (Fig. 5E) and a MLD of approximately 10 m (Fig. 5C). Although we expected that reduced light availability beneath the 0.77 ± 0.09 m thick first-year ice at the edge of the SIZ would result in lower phytoplankton abundance, water column Chl *a* continued to increase as we traveled further into the ice pack (Fig. 2B). Between stations 52 and 56, depth-integrated phytoplankton biomass beneath the sea ice rose from 212 mg Chl *a* m^{-2} (8.8 g C, m^{-2}) to a remarkable 1016 mg Chl *a* m^{-2} (28.7 g C m^{-2}) at station 56 (Fig. 6A), despite sea ice cover of 100% and an increase in sea ice thickness to 1.03 ± 0.15 m (Table 1). Most of this phytoplankton biomass was within the upper 30 m of the water column, with the highest Chl *a* concentrations near the ice/seawater interface (Fig. 5B). The depth over which this bloom extended (30–70 m) and the high depth integrated phytoplankton biomass distinguishes this under-ice bloom from the much smaller blooms that have been observed previously in shallow meltwater lenses beneath the ice that only extend ~1 m below the ice water interface (Gradinger, 1996; Spilling, 2007). The ship's underway fluorometer showed that this massive diatom bloom continued for another 32 km north of station 56 before terminating just north of the shelf break near station 57 (Fig. 2B). In total, the under-ice phytoplankton bloom along Transect 1 extended for ~105 km from the ice edge to the shelf break. Diatoms were the most abundant phytoplankton group beneath the ice, including species in the genera *Chaetoceros*, *Thalassiosira*, and *Fragilariopsis*, and at a few stations, *Odontella* (more details can be found in Laney and Sosik., 2014).

Transect 2, which also terminated north of the shelf break at station 57, was sampled at a higher spatial resolution within the SIZ (Fig. 2A) and exhibited a spatial pattern in phytoplankton biomass that was almost identical to Transect 1. Starting in open water southeast of the SIZ (station 71, Fig. 5H), the SCM was located progressively closer to the surface with proximity to the sea ice edge (station 66, Fig. 5I) and depth-integrated Chl *a* increased dramatically from 54 mg m^{-2} to 576 mg m^{-2} (Fig. 6B). Beneath the ice, phytoplankton biomass increased with distance in from the ice edge despite increasing ice thicknesses (to 1.21 ± 0.10 m, Table 1). Depth-integrated phytoplankton biomass along Transect 2 was even higher than on Transect 1, ranging from 921 to 1292 mg Chl *a* m^{-2} beneath the ice at stations 59–61 (Fig. 6B). The under-ice bloom along Transect 2 extended for ~133 km between the ice edge and its termination at the shelf break.

3.3. Light transmission through sea ice

Vertical light profiles taken through the sea ice at stations 55–57 showed that bare ice transmitted approximately 12.7–17.5% of incident surface light to the water column below (Table 2). Due to the lack of significant snow cover, light attenuation in bare ice was dominated by the presence of a highly scattering surface layer consisting of drained ice crystals. In contrast, the ice beneath melt ponds lacked the surface scattering layer and was thinner than the bare ice (Fig. 4B). Hence, ponded ice transmitted approximately 46.7–58.6% of incident surface light to the underlying water column, 4-fold more than bare ice (Table 2).

Interestingly, the euphotic depth (0.1% of visible incident surface light) associated with both bare and ponded ice at a given station was identical (Table 2). This is because light transmitted to the upper ocean through melt ponds scatters into adjacent areas overlain by bare ice (Fig. 4B). Consequently, with increasing distance below the underside of the ice, the underwater light field became a more uniform mix of light transmitted through both bare ice and melt ponds (Frey et al., 2011).

Euphotic depth did vary by more than a factor of three between stations (Table 2) as a result of changes in light attenuation by particulate and dissolved materials within the water column. For example, beam attenuation at 488 nm increased 6-fold from 0.26 m^{-1} in surface waters outside the ice pack (station 46) to 1.54 m^{-1} within the under-ice phytoplankton bloom (station 56), due to large increases in both particle scattering (5-fold) and particle absorption (3.5-fold). Light absorption within the bloom was almost entirely attributable to particles (91%), mainly phytoplankton (78%), and to a lesser extent by CDOM. The patterns in particle absorption and scattering are consistent with observed differences in particle number (0.9–1.8 × 10^{11} m^{-3}), particle dry mass (0.4–2.7 μg L^{-1}), and particle median diameter (2.2–3.6 μm) between stations (more details can be found in Neukermans et al., 2014). Due to the strong light attenuation within the water column, the euphotic depth shoaled considerably within the under-ice phytoplankton bloom, decreasing from 46 m at station 46 (in open water) to only ~10 m at station 56.

3.4. Dissolved nutrients and gases

Along Transect 1, the nitracline (Fig. 5C) largely tracked the depth of the mixed layer (Fig. 5C) and was deepest in open water southeast of the sea ice edge, extending to ~30 m at station 46. Surface water NO_3 concentrations at this station were below our detection limit (0.01 μmol L^{-1}), increasing to 1.65 μmol L^{-1} at a depth of 27 m and reaching a maximum of 10.5 μmol L^{-1} near the sea floor (44 m). The nitracline shoaled as we approached the ice, reaching ~10 m at the ice edge (station 52), with NO_3 concentrations of 0.3 μmol L^{-1} at the surface and 4.5 μmol L^{-1} at 11 m. Near-bottom NO_3 was also higher at this station (18 μmol L^{-1}) than they were at station 46. The nitracline was shallowest beneath the sea ice, reaching its minimal depth (~7 m) near station 55 (Fig. 5C). The nitracline along Transect 2 exhibited a similar spatial pattern to Transect 1, being deepest in open water southeast of the sea ice edge. Unlike Transect 1, however, the nitricline depth (25–30 m) exceeded the MLD (~10 m) in open water, indicating that the MLD had shoaled after the nitricline had formed (Fig. 5J). Maximum nitracline depths (~40 m) were also

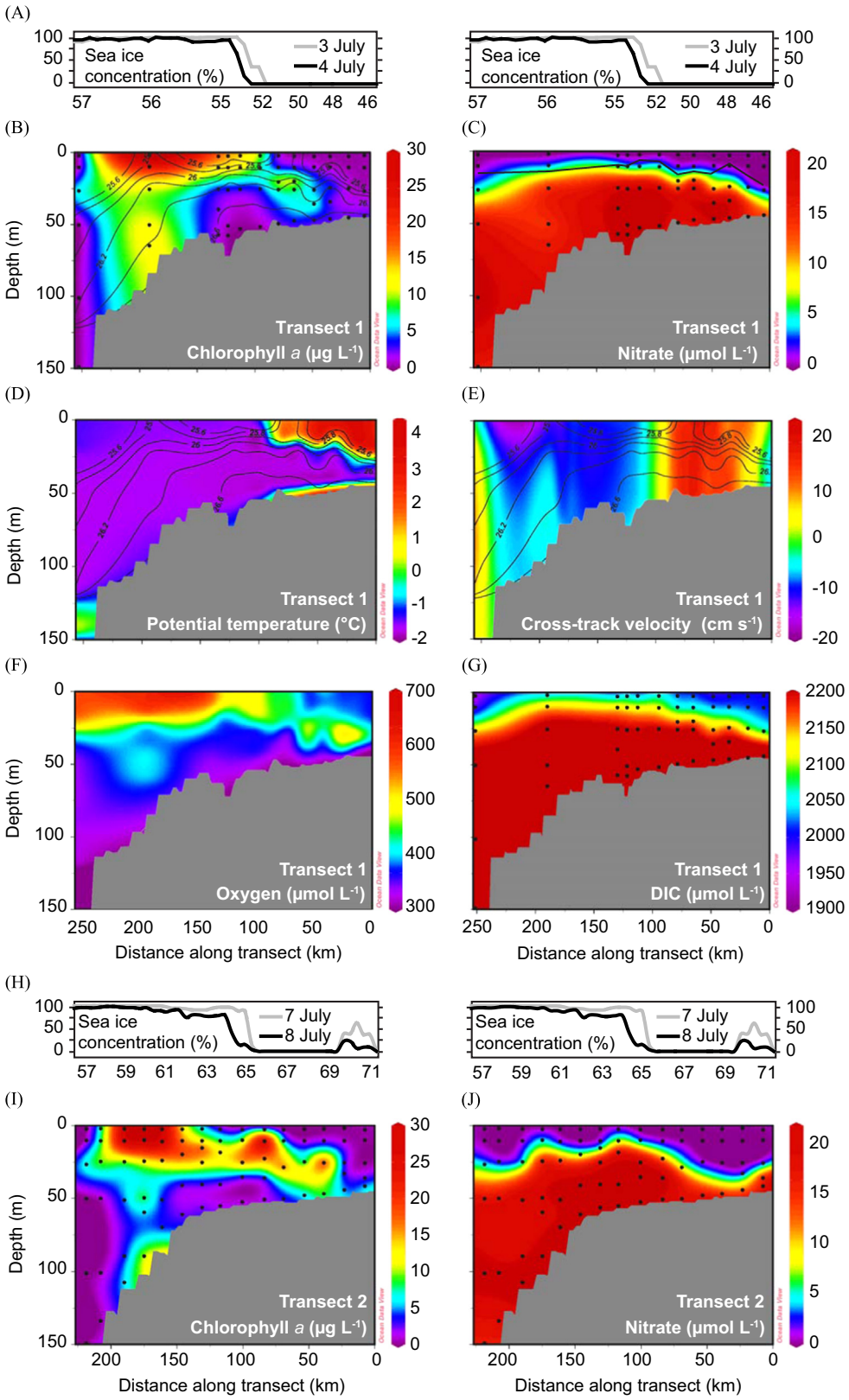

Fig. 5. Hydrographic sections from ICESCAPE 2011 showing under-ice phytoplankton bloom characteristics. (A–G) are from Transect 1 and show (A) sea ice concentration, (B) chlorophyll *a*, (C) nitrate, (D) potential temperature (θ), (E) cross-track velocity (positive values denote northeastward flow), (F) dissolved oxygen, and (G) dissolved inorganic carbon (DIC). (H–J) are from Transect 2 and show concentrations of (H) sea ice, (I), chlorophyll *a*, and (J) nitrate. Station numbers are above each panel and black dots represent sampling depths. Solid contour lines in (B), (D), and (E) are potential density (σ_θ). The black line in (C) and (J) denotes the depth of the mixed layer.

somewhat greater along Transect 2 than on Transect 1, with NO_3 being completely consumed (i.e. below the detection limit) to a depth of 26 m at stations 69 and 70. The nitracline again shoaled with proximity to the ice edge and was shallowest under the ice, although nitracline depths were more spatially variable than along Transect 1.

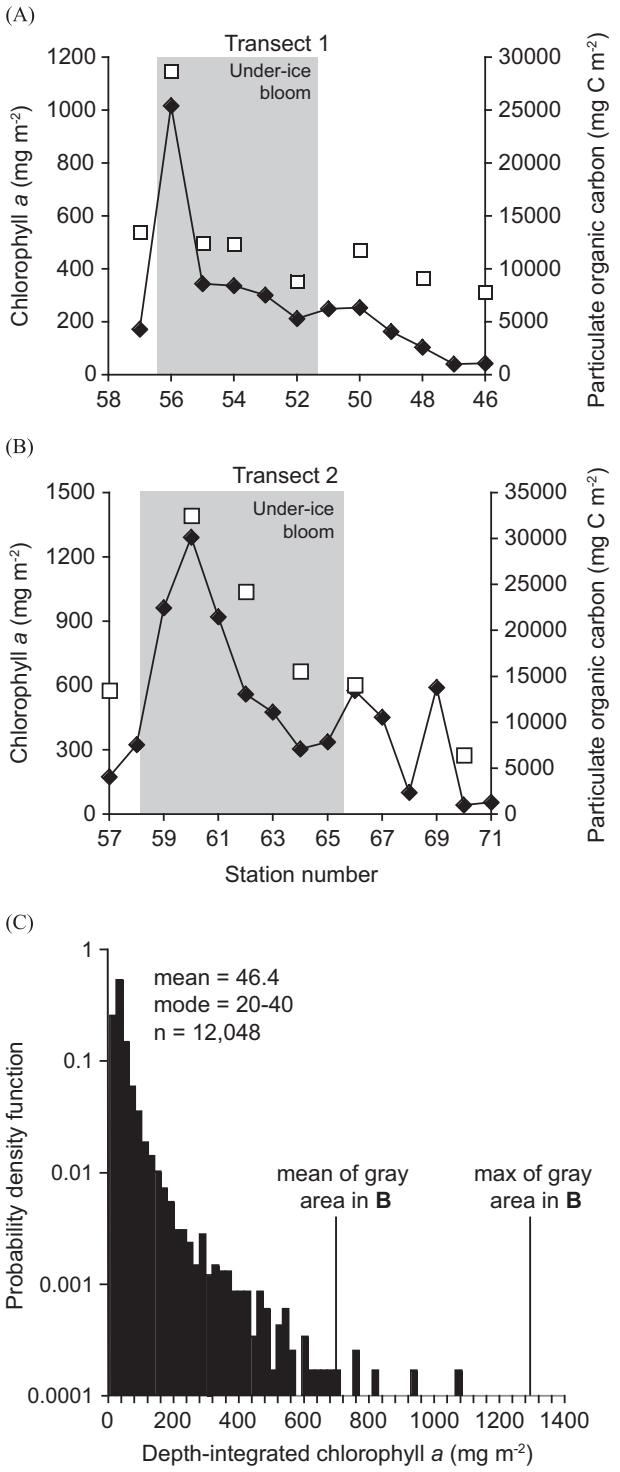

Fig. 6. Depth-integrated chlorophyll *a* (diamonds) and particulate organic carbon (squares) along (A) Transect 1 and (B) Transect 2. Gray areas denote samples collected within the under-ice phytoplankton bloom. Probability density function (C) for depth integrated water column Chl *a* from the global SeaBASS pigment database (http://seabass.gsfc.nasa.gov/). Note log scale of *y*-axis. The mean depth-integrated biomass in the under-ice bloom along Transect 2 ranks in the top 0.1% of global values. Depth-integrated Chl *a* at station 60 is higher than any value in the database.

Dissolved oxygen (O_2) concentrations were very high along both Transect 1 (Fig. 5F) and Transect 2 (not shown). At station 47, located southeast of the ice edge, O_2 concentrations were highest at a depth of 25 m (466.1 μmol L^{-1}), although there was still significant supersaturation in shallower waters. Like Chl *a* and the nitracline, the depth of maximum O_2 concentration shoaled with proximity to the ice edge. Beneath the ice pack, O_2 concentrations were highest in the upper ~25 m of the water column, reaching values as high as 583.1 μmol L^{-1} at the surface of station 61. This station also exhibited enhanced O_2 concentrations down to a depth of approximately 75 m.

Dissolved inorganic carbon (DIC) concentrations in the deep samples along Transect 1 varied from approximately 2250 to 2303 μmol L^{-1}. The DIC depletion pattern (Fig. 5G) strongly resembled that of NO_3, with low DIC values in open surface waters southeast of the sea ice edge (2064–2098 μmol L^{-1} at stations 46–48) and substantial depletion down to at least 30 m. The depth of DIC depletion diminished toward the ice edge, eventually shoaling to ~10 m at ice edge station 52. There was less DIC depletion in waters beneath the sea ice (except station 57), with surface DIC values reduced to 2105–2190 μmol L^{-1} at stations 52–55.

Table 2
Optical characteristics[a] at sea ice stations associated with under-ice phytoplankton bloom.

Station	Ice thickness (m)	Light transmittance (%)		Euphotic depth (m)	
		Bare ice	Ponded ice	Bare ice	Ponded ice
55	0.77 ± 0.09	17.5 ± 0.7	53.8 ± 1.3	17.5 ± 0.06	17.9 ± 0.40
56	1.03 ± 0.15	12.7 ± 0.5	46.7 ± 1.3	10.0 ± 0.03	11.0 ± 0.03
57	1.21 ± 0.10	13.6 ± 0.7	58.6 ± 1.2	32.4 ± 0.43	33.2 ± 1.01

Euphotic depth includes thickness of overlying sea ice.
Three light casts were done at each station.
[a] Mean ± standard deviation

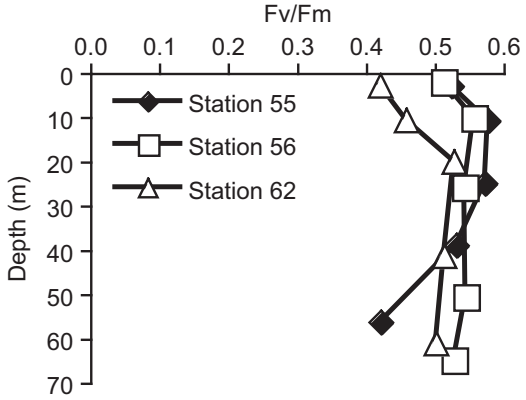

Fig. 7. Depth profiles of the efficiency of electron flow through photosystem II (Fv/Fm) within the under-ice phytoplankton bloom. All values exceed 0.4, suggesting that phytoplankton were physiologically competent throughout the water column.

3.5. Phytoplankton photophysiology and growth rate

Microscopic analysis indicated that under-ice phytoplankton at all stations were healthy, with few observations of empty or senescing diatom frustules. This conclusion is supported by observations of generally high efficiency of electron flow through photosystem II (Fv/Fm), which exceeded 0.4 at all depths shallower than 70 m and exceeded 0.5 in 12 out of the 15 samples where Fv/Fm in the under-ice bloom was measured (Fig. 7).

Photosynthetic parameters determined for phytoplankton sampled at the surface and at ~25 m (the approximate depth of the SCM in open water) at a given station were not significantly different (*t*-test, $p > 0.05$) across our study region (Table 3). However, photosynthetic parameters of under-ice phytoplankton differed significantly from those of phytoplankton in nearby open water. The maximum Chl *a*-specific photosynthetic rates (P_m^*) within the under-ice phytoplankton

bloom (1.40 ± 0.33 mg C mg^{-1} Chl a hr^{-1}) were double those of their open water counterparts (0.71 ± 0.14 mg C mg^{-1} Chl a hr^{-1}), despite growing beneath heavy sea ice cover (t-test, $p < 0.05$). Similarly, the photosynthetic efficiency (α^*) of under-ice phytoplankton was twice as large that of their open water counterparts (t-test, $p < 0.05$), averaging 0.024 ± 0.007 and 0.012 ± 0.004 mg C mg^{-1} Chl a hr^{-1} (μmol photons m^{-2} s^{-1})$^{-1}$, respectively (Table 3). The mean photoacclimation parameter (E_k) for the under-ice bloom (61.2 ± 18.0 μmol photons m^{-2} s^{-1}) was not significantly different (t-test, $p > 0.05$) from that of phytoplankton growing in open waters (66.0 ± 26.6 μmol photons m^{-2} s^{-1}). The high P_m^*, high α^*, and low E_k indicate that the under-ice phytoplankton were well adapted to grow at the reduced light levels encountered below the Arctic ice pack.

The largest physiological difference between the under-ice phytoplankton and their open water counterparts is their maximum biomass-specific growth rate, calculated from both short-term estimates of P–E parameters and from 24-h NPP measurements. Light-saturated growth rates (near the ice/water interface) within the under-ice bloom along Transect 1 were extraordinarily high, ranging from 0.86 d^{-1} near the ice edge to 1.59 d^{-1} at the high-biomass station 56. Light-saturated growth rates along Transect 2 were somewhat lower but still very high, varying from 0.21–1.20 d^{-1}. Five of the eight stations associated with the under-ice bloom exhibited phytoplankton light-saturated growth rates > 1.0 d^{-1}, which are much higher than expected for polar waters near the freezing point of -1.8 °C (0.53 d^{-1}, Eppley, 1972).

The mean light-saturated growth rate within the under-ice bloom was 0.89 d^{-1} (Table 3), approximately 6-fold higher than the mean growth rate of phytoplankton collected in open water (0.15 d^{-1}). This large difference is due in part to the elevated POC concentration associated with a higher detrital content in the older open water phytoplankton blooms (μ=NPP/POC or $P^* \cdot$ Chl a/POC). However, it is also a reflection of the fact that phytoplankton growing in open waters had already consumed much of the NO_3 in near surface waters by the time of our cruise and were concentrated at the sub-surface nitracline where both nutrients and light levels are relatively low. In contrast, phytoplankton growing beneath the ice had not yet consumed all of the available nutrients from within the euphotic zone and were able to maintain much higher growth rates.

Table 3
Photosynthetic Parameters of Phytoplankton at the surface and the SCM from the under-ice bloom (bloom) and adjacent open water (non-bloom).

	P_m^*	α^*	E_k	μ
Surface				
Bloom	1.35 (0.30)	0.021 (0.006)	67.6 (22.4)	0.85 (0.47)
Non-bloom	0.68 (0.11)	0.011 (0.003)	67.9 (25.1)	0.05 (0.02)
SCM				
Bloom	1.45 (0.38)	0.027 (0.007)	54.9 (10.0)	0.92 (0.30)
Non-bloom	0.74 (0.17)	0.013 (0.005)	64.0 (31.9)	0.24 (0.23)
All				
Bloom	1.40 (0.33)	0.024 (0.007)	61.2 (18.0)	0.89 (0.39)
Non-bloom	0.71 (0.14)	0.012 (0.004)	66.0 (26.6)	0.15 (0.18)

[a] Mean ± standard deviation.
P_m^* – mg C mg^{-1} Chl a hr^{-1}, α^* – mg C mg^{-1} Chl a hr^{-1} (μmol photons m^{-2} s^{-1})$^{-1}$, E_k – μmol photons m^{-2} s^{-1}, μ – d^{-1}.
Bloom stations: 52, 54, 55, 56, 58, 60, 62, and 64. Non-bloom stations: 46, 48, 57, and 70.

4. Discussion

4.1. Phytoplankton under the ice

It is noteworthy that the mean biomass associated with the under-ice phytoplankton bloom we observed during ICESCAPE 2011 was comparable to depth-integrated values from the most productive pelagic ecosystems in the global ocean. In fact, the maximum depth-integrated biomass we measured at station 60 was higher than any of the 12,048 open ocean values currently contained in the SeaBASS pigment database managed by NASA (Fig. 6C). Although these high biomass levels were observed deep within the ice pack under relatively thick (0.8–1.2 m) ice, it is important to determine whether this bloom (1) originated as a sea ice microalgal bloom that was subsequently released into the water column, (2) advected beneath the ice from the site of an earlier MIZ bloom, or (3) developed exclusively beneath the ice.

The majority of the stations within the under-ice the bloom were overwhelmingly ($> 80\%$ by cell cross-sectional area) dominated by pelagic diatoms of the genera *Chaetoceros*, *Thalassiosira*, and *Fragilariopsis*, indicating that this was not a remnant sea ice algal bloom that had sloughed off into the water column, although the diatom *Odontella aurita* was abundant at station 56 and is occasionally found in sea ice (McMinn et al., 2008). This conclusion is further supported by the coincidence of extraordinarily high algal biomass and large nutrient deficits in the upper 25–30 m of the water column beneath the ice, which can only be the result of nutrient uptake by phytoplankton growing within the water column. Sea ice algae simply cannot deplete nutrients from that far below the ice/water interface. It is possible that algae released from the sea ice may have helped to seed the under-ice phytoplankton bloom, although we measured very low ice algal biomass during our study.

The most intense phytoplankton blooms previously reported in polar waters were generally associated with open waters along the MIZ (Alexander and Niebauer, 1981; Sakshaug, 2004; Perrette et al., 2011), where meltwater-induced surface stratification creates light conditions that are favorable for phytoplankton growth. Occasionally, these MIZ blooms can become ice covered if either sea ice advances back into waters where a MIZ bloom has already developed (Mundy et al., 2009) or local circulation advects the MIZ bloom beneath the ice pack. As a result, it is important to distinguish ice-covered MIZ blooms from phytoplankton blooms that develop entirely beneath the sea ice. On the basis of age and location of the bloom relative to both the ice edge and bottom topography, and nutrient and biogenic gas concentrations beneath the ice and in the adjacent open water, we determined that the under-ice phytoplankton bloom we observed during ICESCAPE 2011 was neither a residual MIZ bloom nor an open water bloom that had been transported beneath the ice.

First, satellite observations show that the sea ice in the Chukchi Sea consistently retreated in a northwestward direction prior to our sampling the bloom, ruling out the possibility that ice had ever reversed direction and drifted over a previously developed MIZ bloom. Second, phytoplankton biomass associated with the under-ice bloom along both Transect 1 and 2 reached its maximum value approximately 120 km from the ice edge at a location where nutrients were enhanced due to shelf break upwelling from depth (see below). This bathymetric constraint strongly supports the conclusion that the bloom developed beneath the ice, with its northwestern boundary (the boundary located deepest within the ice pack) controlled by the position of the shelf break.

Finally, if the bloom had advected beneath the ice from open water, it would have been in a much later stage of development than we observed, given the high growth rate of the phytoplankton beneath the ice and the local circulation patterns. The shortest route from ice-free waters to our study region beneath the ice would require advection of the bloom to the northwest in the direction of sea ice motion. This is unlikely since no known currents in the vicinity of our study region flow from the southeast to the northwest. Instead, one current flows northward through Central Channel then northeastward around Hanna Shoal while

another flows either eastward from Herald Canyon along the shelf break (Pickart et al., 2010) or in the opposite direction when the shelf-break jet is reversed. Furthermore, maximum current velocities in the region measured by ADCP are approximately 15 cm s^{-1} (13 km d^{-1}), barely fast enough to keep up with the rate of sea ice retreat (11 km d^{-1}). Thus, even if the flow was in the same direction as the retreating sea ice, the bloom would be advected beneath the ice at a net rate of at most 2 km d^{-1}. Given that the far end of the bloom at station 56 was approximately 120 km from the ice edge at the time of sampling (and even farther from the edge prior to sampling), the bloom would have taken at least 60 days to advect from the ice edge to its observed position. Because surface water nitrate had not yet been entirely depleted under the ice and there was limited evidence of vertical export of senescent phytoplankton cells to the sediments despite the shallow water depth (microscopic analysis showed that the few cells reaching the sediments appeared young and healthy), it is extremely unlikely that the bloom was >60 days old. Even this estimate of the bloom age is conservative because it assumes that the bloom advected beneath the ice by the shortest route possible. Advection from any other direction (especially the directions of the prevailing currents, Fig. 5E) would require the bloom to move a much longer distance from a region of ice-free water into our study area and be much older than 60 days when we sampled it. Therefore, we are confident that the phytoplankton bloom developed recently beneath the ice in the location where we sampled it rather than being advected in from elsewhere.

Rather than the under-ice phytoplankton bloom being a remnant MIZ bloom that had developed previously in ice-free waters, evidence from ICESCAPE suggests that the SCM we observed in open waters of the MIZ along both Transects 1 and 2 represents the later stages of the under-ice phytoplankton bloom. The distributions of Chl *a*, nutrients, and biogenic gases along both ICESCAPE 2011 transects, as well as the general retreat of sea ice from the southeast to the northwest (Fig. 2A), indicate that the phytoplankton bloom was progressively older towards the southeast end of both transects. For example, stations 46 and 47 exhibited a deep nutricline (Fig. 5C,J) and both had high surface oxygen (Fig. 5F) and low DIC concentrations (Fig. 5G) despite little particulate organic material in the water column. This suggests that the phytoplankton that had previously bloomed in these waters had been either exported to the sediments or grazed. Moving closer to the ice edge, both the SCM (Fig. 5B,I) and the nitracline (Fig. 5C,J) became progressively shallower, indicative of a bloom at an increasingly earlier stage of development. Furthermore, satellite-based sea ice distributions show that the stations along Transect 1 and 2 located in open water near the ice edge were covered by ice a few days prior to sampling. Thus, the southeastern portions of both transects that were in open water at the time of sampling likely harbored remnant phytoplankton blooms that had developed weeks earlier when the region was still ice-covered and had subsequently retreated downward as surface nutrients were depleted.

4.2. Shelf break upwelling

Most of the horizontal extent of the under-ice phytoplankton bloom observed during ICESCAPE likely subsisted on the substantial amount of WW nutrients residing on the shelf (e.g. those that are mixed into surface waters during winter convection). However, wind-forced upwelling appears to have tapped an additional reservoir of nutrients in the shelf break jet, resulting in the highest depth-integrated Chl *a* along both Transect 1 (station 56) and Transect 2 (Station 60) (Fig. 5B,I) and among the highest measured anywhere in the global ocean (Fig. 6C). For much of the month preceding our measurements, winds in the region were easterly between 5–10 m s^{-1} (Spall et al., 2014). Under such wind forcing, the shelfbreak jet in the Beaufort Sea typically reverses (i.e. flows to the west, Schulze and Pickart, 2012). In both of our Chukchi Sea transects during ICESCAPE 2011, the shelf break jet was also reversed and isopycnals extended from deeper offshore at station 57 to the surface layer near the shelf break (Fig. 5D,E), the classic signature of upwelling. As detailed in Spall et al. (2014) the upwelling at the shelfbreak results because of the overlapping surface and bottom boundary layers on the shallow Chukchi shelf. This reduces the offshore Ekman transport on the shelf relative to that over the deeper slope (where the two boundary layers do not overlap). The resulting divergence in Ekman transport leads to the upward velocities at the shelfbreak, which, together with wind mixing in the upper layer, provides a mechanism for replenishing surface water nutrients near the shelf break. It is important to note that the presence of pack-ice does not prohibit upwelling; even with 100% ice cover, stress is imparted to the water column by the mobile ice. Schulze and Pickart (2012) found that the upwelling response was similar for a complete ice cover compared to that for ice-free conditions. The amount of additional NPP on the Chukchi shelf that is generated by upwelling at the ice-covered shelf break warrants further investigation.

The enhancement of blooms at the continental shelf break may become more common in years to come. Under a warming climate, high latitude storms (i.e. northward-tracking Aleutian lows) are predicted to become more frequent and stronger (Zhang et al., 2004; Sorteberg and Walsh, 2008) and will intensify nutrient upwelling. In addition, analysis of synoptic-scale sea-level pressure fields (NARR data, 1979–2011) indicates that upwelling winds on the northern Chukchi shelf in late spring are significantly correlated with the strength and position of the Beaufort Sea High ($p<0.05$). Since the year 2000, there has been a marked increase in the incidence of such easterly winds, likely related to an intensification and westward movement of the Beaufort Sea High associated with regional warming (Polyakov et al., 2002; Comiso, 2003), which is likely to continue into the future.

4.3. How widespread are under-ice blooms?

Hydrographic and biological data within ice-covered regions of the Arctic Ocean are sparse, making it difficult to assess the spatial distributions of under-ice phytoplankton blooms. Nonetheless, they may have been observed by other expeditions, albeit not to the degree reported here. For instance, phytoplankton biomass beneath ~1.8 m thick ice in Barrow Strait, Canadian Arctic Archipelago in both 1994 and 1995 quickly rose from ~20 to ~300 mg Chl *a* m^{-2} after a period of rapid snow melt in the late spring–early summer, presumably the result of an under-ice phytoplankton bloom (Fortier et al., 2002). Unfortunately this bloom was only documented at a single location and little additional information about the bloom was collected. In the Canadian Beaufort Sea, under-ice primary production that was measured within 1–6 km of the ice edge accounted for 22% of total primary production in the MIZ in 2008 (Mundy et al., 2009), with photosynthetic rates (Palmer et al., 2011) similar to those measured during ICESCAPE 2011. Although it is unknown how far into the pack this enhanced phytoplankton biomass extended, this bloom was likely an actively growing MIZ phytoplankton bloom that had advected beneath the ice and continued to grow on upwelled nutrients. During the spring of 1998 on the Chukchi shelf, high Chl *a* (5–19 mg m^{-3}) and low NO_3 concentrations (<1–7 μmol L^{-1}) were observed in the upper 10–20 m of the water column beneath 1.5 m thick sea ice (Yager et al., 2001). This apparent under-ice bloom was even more extensive than the one reported here, continuing in roughly a north–south direction for ~190 km. However, unlike the under-ice bloom we observed, this

bloom was reported to be dominated by the colonial epontic sub-ice diatom *Melosira arctica*, although some water column species were also present. Finally, a transect from the open ocean to the ice edge in the Barents Sea in 1991 exhibited bloom characteristics similar to those we observed during ICESCAPE 2011. A well-defined SCM in open water became progressively shallower and more intense with proximity to the ice edge, where Chl *a* concentrations reached their highest level at the ocean surface (Strass and Nothig, 1996). Although the sampling vessel was unable to enter the SIZ, the authors speculated that the bloom had been initiated earlier beneath the ice.

At a minimum, measurements made during the first year of our study (ICESCAPE 2010) suggest that under-ice phytoplankton blooms may have been more widespread on the nutrient-rich Chukchi shelf earlier in the season. During ICESCAPE 2010, we observed a similar massive under-ice phytoplankton bloom along our Chukchi North transect at the same location as the bloom seen during ICESCAPE 2011 (Fig. 2A and C), with Chl *a* concentrations in excess of 20 $\mu g\ L^{-1}$ and large surface NO_3 deficits (Fig. 8C). Unfortunately, sampling under the ice never extended more than 10 km from the ice edge (Fig. 8A) so it was not recognized as an under-ice bloom at the time. In addition, the Chukchi South transect sampled further to the south during ICESCAPE 2010 (Fig. 2C) exhibited high near-surface Chl *a* concentrations (Fig. 8D) and large surface deficits in NO_3 (Fig. 8E) and DIC (not shown) within just a few days of becoming ice-free, implying that an under-ice phytoplankton bloom had developed there earlier in the season when the region was still ice-covered. This conclusion is consistent with observations that mean melt pond fraction can exceed 50% of the ice surface area earlier in the season during the initial flooding stage (Polashenski, 2011). Consequently, even more light would have penetrated the ice in the weeks prior to our arrival when the under-ice bloom first began to develop. It should also be noted that despite similar sea ice conditions, parts of the eastern Chukchi Sea dominated by the low-nutrient ACW and adjacent Canada Basin showed no evidence of under-ice phytoplankton blooms during ICESCAPE 2011, highlighting the requirement for an ample nutrient supply. Combined, these results provide hints that under-ice phytoplankton blooms have been observed before and may exist in regions outside of the Chukchi Sea.

The location where under-ice phytoplankton blooms were observed during ICESCAPE in 2010 and 2011 suggests that these blooms require both high nutrient concentrations and ice cover that transmits sufficient light for phytoplankton net photosynthesis. Given the proliferation of first-year ice in recent years (Comiso, 2012), melt ponds are likely to be increasingly widespread. Furthermore, the Arctic Ocean has an enormous continental shelf, ~50% of which has surface NO_3 concentrations above 10 $\mu mol\ L^{-1}$ in early spring (Zhang et al., 2010; Codispoti et al., 2013), making these areas potential sites for large under-ice phytoplankton blooms. Thus, taking into account the extent of the Arctic continental shelf and the proportion of the shelf having high nutrient concentrations, it is possible that conditions may be favorable for under-ice phytoplankton blooms over approximately 25% of the area of the Arctic Ocean.

4.4. Annual net primary production

Because a large area of the Arctic continental shelf has conditions amenable to under-ice phytoplankton blooms, and previous reports have hinted at such blooms in the Barents Sea, Beaufort Sea, and Canadian Arctic Archipelago, and now documented here for the Chukchi Sea, it is likely that these blooms are widespread.

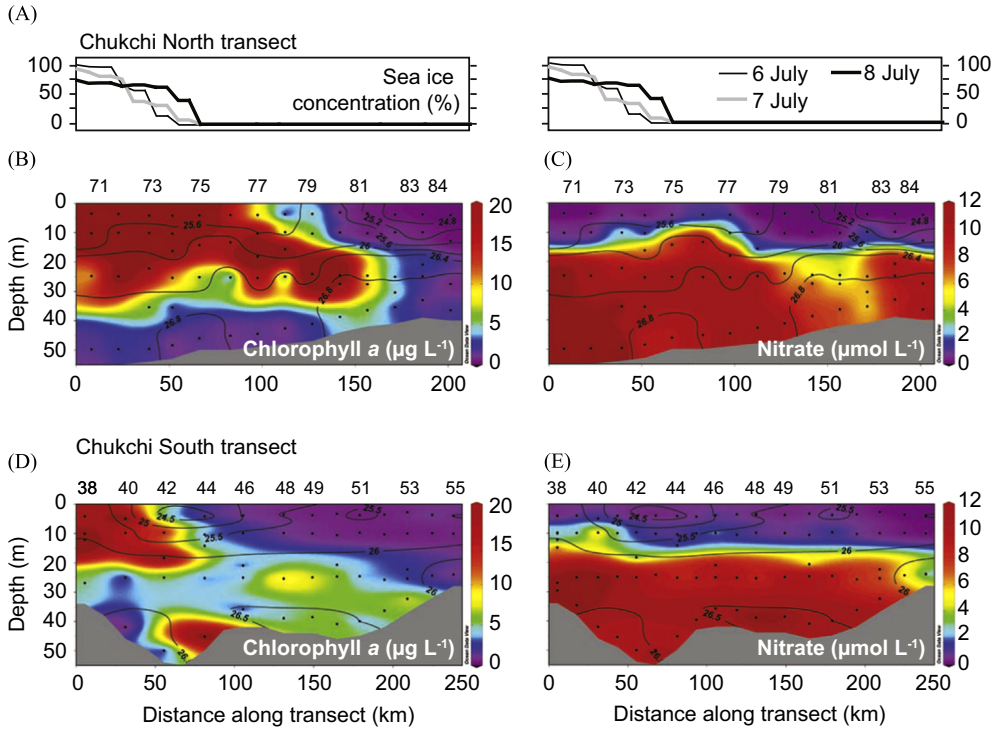

Fig. 8. Additional evidence of under-ice phytoplankton blooms from ICESCAPE 2010. (A) shows the sea ice concentration at the time of sampling. The similarity of this bloom to the under-ice phytoplankton blooms observed during ICESCAPE 2011 was remarkable, with (B) the same extraordinarily high surface Chl *a* concentrations relatively far within the ice pack transitioning to subsurface maxima that gradually deepened toward the open ocean, as surface (C) nitrate was depleted. The Chukchi South transect was located further south but exhibited the same pattern in (D) Chl *a* and (E) nitrate concentration as the Chukchi North transect and both Transect 1 and 2 from ICESCAPE 2011, with high surface Chl *a* concentrations to the west, and a well-developed subsurface Chl *a* maximum (SCM) farther east. Although we sampled this transect while it was ice-free, the western side of the transect had only been ice-free for one day before sampling. Therefore, the large surface phytoplankton bloom on the west side of the transect must have formed when the region was still covered by sea ice.

If so, then current estimates of annual NPP on Arctic continental shelves that are based on phytoplankton production in open water (e.g., Pabi et al., 2008; Arrigo and van Dijken, 2011) may be drastically underestimated. For example, in the same location where the under-ice phytoplankton bloom was observed during ICESCAPE 2011, annual NPP calculated from satellite-derived estimates of surface Chl *a* (satellites cannot detect phytoplankton beneath sea ice) averaged only 5–10 g C m^{-2} yr^{-1} (Arrigo and van Dijken, 2011). However, deficits of DIC and NO_3 in surface waters beneath the sea ice observed during ICESCAPE 2011 yield a production value of ~70 g C m^{-2} between the start of the under-ice phytoplankton bloom and the time of sampling (July 4–8). These very high values are consistent with our measured rates of daily NPP for the under-ice phytoplankton bloom (1.2–4.8 g C m^{-2} d^{-1}) determined from ^{14}C incorporation. Considering that phytoplankton were still blooming beneath the ice at the time of sampling and that nutrient deficits account for only 40–65% of NPP in polar and sub-polar shelf waters (Hansell et al., 1993; Walsh et al., 2005), our results suggest that in areas where under-ice blooms develop, annual rates of NPP beneath the sea ice may be more than an order of magnitude higher than rates of NPP when those waters become ice free. Given that under-ice blooms may be quite widespread, it is imperative that their contribution to pan-Arctic NPP be quantified and added to existing satellite-based estimates of annual NPP in ice-free waters.

4.5. *A new phytoplankton paradigm for the Chukchi sea*

The long-standing paradigm of the Arctic Ocean is one in which phytoplankton proliferate at the ice edge, supplying a substantial fraction of annual NPP (Hameedi, 1978; Perrete et al., 2011) and concentrating much of the food web in the MIZ (Bradstreet and Cross, 1982; Stirling, 1997; Loeng et al., 2005). However, data from ICESCAPE suggest that this scenario needs to be revised for the Chukchi Sea to account for phytoplankton blooms that begin beneath the sea ice.

Phytoplankton growth under the ice in the nutrient-rich Chukchi Sea likely begins soon after the snow cover melts, surface melt ponds form, and light transmission through the ice to the water column increases (Arrigo et al., 2012). Whether this early stage of the bloom is initiated by the release of algae from the sea ice is not known. Eventually, a SCM develops as phytoplankton exhaust nutrients in the upper water column beneath the ice. When the sea ice finally melts and the water column becomes stratified, nutrient-poor surface waters become isolated from nutrient-rich waters below, preventing the development of a classic MIZ bloom (Alexander and Niebauer, 1981). On the other hand, phytoplankton growing beneath the ice are already acclimated to low light conditions, resulting in higher growth rates in the open water SCM (Palmer et al., 2014). Thus, phytoplankton blooms beneath the Arctic ice pack transform the MIZ from a highly productive surface environment to one where nutrients have been exhausted weeks earlier and the bulk of the algal biomass is located 20–30 m below the surface (Fig. 5B,I). In addition, Arctic sea ice is retreating 2.4 days earlier each year (Arrigo and van Dijken, 2011), accelerating the development of open water phytoplankton blooms (Kahru et al., 2011). The implications of this marked shift in the timing and location of peak NPP in Arctic waters are unclear but potentially profound.

Many organisms time their migrations and reproduction cycle to coincide with peak Arctic NPP (Loeng et al., 2005; Soreide et al., 2010; Wassmann et al., 2010; Wassmann, 2011) so altering the location and timing of the spring bloom could disrupt life cycle strategies that have evolved over millenia (Moore and Huntington, 2008). Furthermore, because these under-ice blooms develop in such cold water, their proliferation could intensify the mismatch between phytoplankton and their zooplankton grazers (Conover and Huntley, 1991), ultimately decreasing the food available to fish, birds, and mammals (Loeng et al., 2005; Bradstreet and Cross 1982) and increasing organic matter export to the sediments (Wassmann et al., 1996) in a region already distinguished by tremendous benthic biomass (Grebmeier et al., 1995).

5. Conclusions

Whether under-ice phytoplankton blooms are a relatively recent phenomenon or whether they have been going on undetected for many years is not known. We do know that in the early 1980s, the location of the under-ice phytoplankton blooms identified during ICESCAPE 2011 remained covered throughout the summer by multi-year ice (Fig. 9). This ice was on average thicker

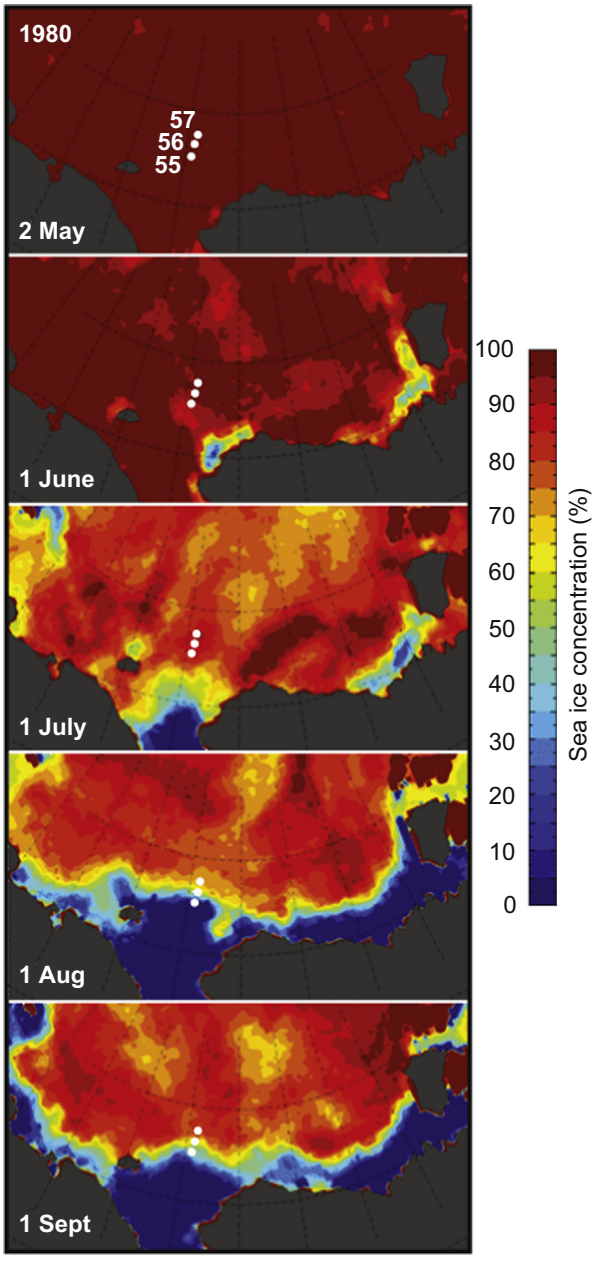

Fig. 9. Time series of sea ice concentration from the spring and summer of 1980. Note that our ICESCAPE 2011 stations 55–57 would have been in ice covered waters throughout the year in 1980 (numbered white dots in upper panel). This was also true of 1981 and 1983. In 1982 and 1984, station 55 was free of ice for only short time at the end of the summer melt season; the other stations remained ice-covered all year.

(~3 m) with a deeper snow cover (0.4 m) and fewer melt ponds than the first year ice we sampled during ICESCAPE. Given the optical properties typical of sea ice and snow (Perovich, 1990), the amount of light transmitted through snow-covered multi-year ice in the 1980s (< 0.1% of surface light) would have been far less than that measured during ICESCAPE 2011 (13–59% of surface light) and inadequate to support a large under-ice phytoplankton bloom. Thus, the area suitable for such blooms in the Chukchi Sea has increased as the proportion of multi-year ice has diminished and melt pond fraction has increased (Lee et al., 2011). However, first-year ice was still relatively widespread on many of the Arctic continental shelves in the past and could have supported under-ice phytoplankton blooms. Whether or not they did remains an open question.

Regardless of whether or not under-ice blooms are a recent phenomenon, the notion that phytoplankton can bloom so explosively under a concentrated ice pack > 1 m thick represents a fundamental shift in the way Arctic marine ecosystems are viewed. Our results show that seasonally ice covered waters on the Arctic continental shelf have the potential to support vastly higher rates of NPP than has been attributed to them in the past. The under-ice water column on the continental shelf appears to be an excellent habitat for phytoplankton blooms to develop due to (1) high nutrient concentrations, (2) moderate light transmission through relatively thin sea ice with a high melt pond fraction, (3) cold under-ice temperatures that may minimize zooplankton grazing, and possibly to (4) attenuation of ultraviolet radiation by sea ice (Frey et al., 2011). Furthermore, the presence of under-ice phytoplankton blooms shifts maximum nutrient consumption and carbon production to earlier in the season and deeper within the pack, with unknown ecological consequences. Much work is still required to determine how widespread under-ice phytoplankton blooms are and how they impact local and regional marine ecosystems. This is particularly important if we are to predict the biological and biogeochemical impacts of further changes in the Arctic Ocean physical environment.

Acknowledgments

This research was supported by the Ocean Biology and Biogeochemistry Program and the Cryosphere Science Program of the National Aeronautic and Space Administration (NNX10AF42G to K. Arrigo, R. Pickart, and J. Swift, NNH10A017I to D. Perovich, NNX10AT67G to W. Balch, NNX10AG36G to N. Bates and J. Mathis, NNX09AE42G and NNX11AF65G to B. G. Mitchell and C. Benitez-Nelson, NNX10AH71G to K. Frey, NNX10AG07G to S. Laney and H. Sosik, and NNX10AG05G to R. Reynolds) and by the Malina project. We would like to thank the captain and crew of the USCGC Healy.

References

Alexander, V., Niebauer, H.J., 1981. Oceanography of the eastern Bering Sea ice-edge zone in spring. Limnol. Oceanogr. 26 (6), 1111–1125.
Armstrong, F.A.J., Stearns, C.R., Strickland, J.D.H., 1967. The measurement of upwelling and subsequent biological processes by means of the Technicon Autoanalyzer and associated equipment. Deep-Sea Res. 14, 381–389.
Arrigo, K.R., van Dijken, G.L., 2011. Secular trends in Arctic Ocean net primary production. J. Geophys. Res. 116, C09011.
Arrigo, K.R., Mills, M.M., Kropuenske, L.R., van Dijken, G.L., Alderkamp, A.-C., Robinson, D.H., 2010. Photophysiology in two major Southern Ocean phytoplankton taxa: photosynthesis and growth of *Phaeocystis antarctica* and *Fragilariopsis cylindrus* under different irradiance levels. Integr. Comp. Biol. 50, 950–966.
Arrigo, K.R., Perovich, D.K., Pickart, R.S., Brown, Z.W., van Dijken, G.L., Lowry, K.E., Mills, M.M., Palmer, M.A., Balch, W.M., Bahr, F., Bates, N.R., Benitez-Nelson, C., Bowler, B., Brownlee, E., Ehn, J.K., Frey, K.E., Garley, R., Laney, S.R., Lubelczyk, L., Mathis, J., Matsuoka, A., Mitchell, B.G., Moore, G.W.K., Ortega-Retuerta, E., Pal, S., Polashenski, C.M., Reynolds, R.A., Scheiber, B., Sosik, H.M., Stephens, M., Swift, J.H., 2012. Massive phytoplankton blooms under Arctic sea ice. Science 336, 1408.
Bates, N.R., Best, M.H.P., Hansell, D.A., 2005. Spatio-temporal distribution of dissolved inorganic carbon and net community production in the Chukchi and Beaufort Seas. Deep-Sea Res., Part II 52 (24-26), 3303–3323, http://dx.doi.org/10.1016/j.dsr2.2005.10.005.
Bradstreet, M.S.W., Cross, W.E., 1982. Trophic relationships at high Arctic ice edges. Arctic 35 (1), 1–12.
Carmack, E., Wassmann, P., 2006. Food webs and physical–biological coupling on pan-Arctic shelves: unifying concepts and comprehensive perspectives. Prog. Oceanogr. 71 (2-4), 446–477, http://dx.doi.org/10.1016/j.pocean.2006.10.004.
Coachman, L.K., Aagaard, K., Tripp, R.B., 1975. Bering Strait: The Regional Physical Oceanography. University of Washington Press, Seattle, Washington.
Codispoti, L.A., Flagg, C., Kelly, V., Swift, J.H., 2005. Hydrographic conditions during the 2002 SBI process experiments. Deep-Sea Res., Part II 52 (24-26), 3199–3226.
Codispoti, L.A., Kelly, V., Thessen, A., Matrai, P., Suttles, S., Hill, V., Steele, M., Light, B., 2013. Synthesis of primary production in the Arctic Ocean: III. Nitrate and phosphate based estimates of net community production. Prog. Oceanogr., 1–25, http://dx.doi.org/10.1016/j.pocean.2012.11.006.
Comiso, J.C., 2003. Warming trends in the Arctic from clear sky satellite observations. J. Climate 16 (21), 3498–3510.
Comiso, J.C., Parkinson, C.L., Gersten, R., Stock, L., 2008. Accelerated decline in the Arctic sea ice cover. Geophys. Res. Lett. 35, L01703.
Comiso, J.C., 2012. Large decadal decline of the Arctic multiyear ice cover. J. Climate 25, 1176–1193.
Conover, R.J., Huntley, M., 1991. Copepods in ice-covered seas – distribution, adaptations to seasonally limited food, metabolism, growth patterns and life cycle strategies in polar seas. J. Mar. Syst. 2, 1–41.
Cooper, L.W., Whitledge, T.E., Grebmeier, J.M., Weingartner, T., 1997. The nutrient, salinity, and stable oxygen isotope composition of Bering and Chukchi Seas waters in and near the Bering Strait. J. Geophys. Res. 102 (C6), 12563–12573.
Cota, G.F., Pomeroy, L.R., Harrison, W.G., Jones, E.P., Peters, F., Sheldon, W.M., Weingartner, T.R., 1996. Nutrients, primary production and microbial heterotrophy in the southeastern Chukchi Sea: Arctic summer nutrient depletion and heterotrophy. Mar. Ecol. Prog. Ser. 135 (1-3), 247–258.
Coupel, P., Jin, H.Y., Joo, M., Horner, R., Bouvet, H.A., Sicre, M.A., Gascard, J.C., Chen, J.F., Garcon, V., Ruiz-Pino, D., 2012. Phytoplankton distribution in unusually low sea ice cover over the Pacific Arctic. Biogeosciences 9 (11), 4835–4850.
Cullen, J.J., Davis, R.F., 2003. The blank can make a big difference in oceanographic measurements. Limnol. Oceanogr. Bull. 12, 29–35.
Dunton, K.H., Goodall, J.L., Schonberg, S.V., Grebmeier, J.M., Maidment, D.R., 2005. Multi-decadal synthesis of benthic–pelagic coupling in the western arctic: role of cross-shelf advective processes. Deep-Sea Res., Part II 52 (24–26), 3462–3477.
Eicken, H., Tucker, W.B., Perovich, D.K., 2001. Indirect measurements of the mass balance of summer Arctic sea ice with an electromagnetic induction technique. Annals Glaciol. 33, 194–200, http://dx.doi.org/10.3189/172756401781818356.
Eppley, R.W., 1972. Temperature and phytoplankton growth in the sea. Fish. Bull. 70 (4), 1063–1085.
Fortier, M., Fortier, L., Michel, C., Legendre, L., 2002. Climatic and biological forcing of the vertical flux of biogenic particles under seasonal Arctic sea ice. Mar. Ecol. Prog. Ser. 225, 1–16.
Frey, K.E., Perovich, D.K., Light, B., 2011. The spatial distribution of solar radiation under a melting Arctic sea ice cover. Geophys. Res. Lett. 38, L22501, http://dx.doi.org/10.1029/2011GL049421.
Gradinger, R., 1996. Occurrence of an algal bloom under Arctic pack ice. Mar. Ecol. Prog. Ser. 131, 301–305.
Gradinger, R., 2009. Sea-ice algae: Major contributors to primary production and algal biomass in the Chukchi and Beaufort Seas during May/June 2002. Deep-Sea Res., Part II 56 (17), 1201–1212.
Grebmeier, J.M., Smith, W.O., Conover, R.J., 1995. Biological processes on Arctic continental shelves: ice-ocean-biotic interactions. In: Smith, W.O., Grebmeier, J. M. (Eds.), Arctic Oceanography: Marginal Ice Zones and Continental Shelves. Coastal and Estuarine Studies, American Geophysical Union, Washington, DC., pp. 231–261.
Grebmeier, J.M., Cooper, L.W., Feder, H.M., Sirenko, B.I., 2006. Ecosystem dynamics of the Pacific-influenced Northern Bering and Chukchi Seas in the Amerasian Arctic. Prog. Oceanogr. 71 (2–4), 331–361, http://dx.doi.org/10.1016/j.pocean.2006.10.001.
Hameedi, M.J., 1978. Aspects of water column primary productivity in the Chukchi Sea during summer. Mar. Biol. 48 (1), 37–46.
Hansell, D.A., Whitledge, T.E., Goering, J.J., 1993. Patterns of nitrate utilization and new production over the Bering-Chukchi shelf. Cont. Shelf Res. 13, 601–627.
Hewes, C.D., Holm-Hansen, O., 1983. A method for recovering nanoplankton from filters for identification with the microscope: the filter-transfer-freeze (FTF) technique. Limnol. Oceanogr. 28, 389–394.
Hill, V., Cota, G., 2005. Spatial patterns of primary production on the shelf, slope and basin of the Western Arctic in 2002. Deep-Sea Res., Part II 52, 3344–3354.

Holm-Hansen, O., Lorenzen, C.J., Holmes, R.W., Strickland, J.D.H., 1965. Fluorometric determination of chlorophyll. ICES J. Mar. Sci. 30, 3–15.
Kahru, M., Brotas, V., Manzano-Sarabia, M., Mitchell, B.G., 2011. Are phytoplankton blooms occurring earlier in the Arctic? Glob. Change Biol. 17, 1733–1739.
Kolber, Z.S., Prasil, O., Falkowski, P.G., 1998. Measurements of variable chlorophyll fluorescence using fast repetition rate techniques: defining methodology and experimental protocols. Biochim. Biophys. Acta Bioenerg. 1367, 88–106.
Laney, S.R., Sosik, H.M., 2014. Phytoplankton assemblage structure in and around a massive under-ice bloom in the Chukchi Sea. Deep-Sea Res. II 105, 30–41, http://dx.doi.org/10.1016/j.dsr2.2014.03.012.
Lee, S.H., Whitledge, T.E., Kang, S.-H., 2007. Recent carbon and nitrogen uptake rates of phytoplankton in Bering Strait and the Chukchi Sea. Cont. Shelf Res. 27 (17), 2231–2249.
Lee, S.H., McRoy, C.P., Joo Lee, H.M., Gradinger, R., Cui, X.H., Yun, M.S., Chung, K.H., Kang, S.H., Kang, C.K., Choy, E.J., Son, S.H., Carmack, E., Whitledge, T.E., 2011. Holes in progressively thinning Arctic sea ice lead to new ice algae habitat. Oceanography 24, 302–308.
Lee, S.H., Joo, H.M., Liu, Z.L., Chen, J.F., He, J.F., 2012. Phytoplankton productivity in newly opened waters of the Western Arctic Ocean. Deep-Sea Res., Part II 81-84, 18–27.
Lewis, M.R., Smith, J.C., 1983. A small volume, short incubation-time method for measurement of photosynthesis as a function of incident irradiance. Mar. Ecol. Prog. Ser. 13, 99–102.
Loeng, H., Brander, K., Carmack, E., Denisenko, S., Drinkwater, K., Hansen, B., Kovacs, K., Livingston, P., McLaughlin, F., Sakshaug, E., 2005. Marine systems, Arctic Climate Impact Assessment. Cambridge Univ. Press, Cambridge, U.K., pp. 453–538.
Lowry, K.E., van Dijken, G.L., Arrigo, K.R., 2014. Evidence of under-ice phytoplankton blooms in the Chukchi Sea from 1998 to 2012. Deep-Sea Res. II 105, 105–117, http://dx.doi.org/10.1016/j.dsr2.2014.03.013.
Maslanik, J., Stroeve, J., Fowler, C., Emery, W., 2011. Distribution and trends in Arctic sea ice age through spring 2011. Geophys. Res. Lett. 38, L13502.
McMinn, A., Hattori, H., Hirawake, T., Iwamota, A., 2008. Preliminary investigation of Okhotsk Sea ice algae; taxonomic composition and photosynthetic activity. Polar Biol. 31 (8), 1011–1015.
Mitchell, B.G., 1990. Algorithms for determining the absorption coefficient of aquatic particulates using the quantitative filter technique (QFT). Proc. Int. Soc. Opt. Eng. 10, 137–148.
Moore, S.E., Huntington, H.P., 2008. Arctic marine mammals and climate change: impacts and resilience. Ecol. Appl. Suppl. 18, S157–S165.
Mundy, C.J., Gosselin, M., Ehn, J., Gratton, Y., Rossnagel, A., Barber, D.G., Martin, J., Tremblay, J.-E., Palmer, M., Arrigo, K.R., Darnis, G., Fortier, L., Else, B., Papakyriakou, T., 2009. Contribution of under-ice primary production to an ice-edge upwelling phytoplankton bloom in the Canadian Beaufort Sea. Geophys. Res. Lett. 36, L17601.
Neukermans, G., Reynolds, R.A., Stramski, D., 2014. Contrasting inherent optical properties and particle characteristics between an under-ice phytoplankton bloom and open water in the Chukchi Sea. Deep-Sea Res. II 105, 59–73, http://dx.doi.org/10.1016/j.dsr2.2014.03.014.
Nghiem, S.V., Rigor, I.G., Perovich, D.K., Clemente-Colon, P., Weatherly, J.W., Neumann, G., 2007. Rapid reduction of Arctic Perennial Sea Ice 34, L19504Geophys. Res. Lett. 34, L19504.
Olson, R.J., Sosik, H.M., 2007. A submersible imaging-in-flow instrument to analyze nano- and microplankton: Imaging FlowCytobot. Limnol. Oceanogr. Methods 5, 195–203.
Ortega-Retuerta, E., Fichot, C.G., Arrigo, K.R., van Dijken, G.L., Joux, F., 2014. Response of marine bacterioplankton to a 1 massive under-ice phytoplankton bloom in the Chukchi Sea (Western Arctic Ocean). Deep-Sea Res. II 105, 74–84, http://dx.doi.org/10.1016/j.dsr2.2014.03.015.
Overland, J.E., Roach, A.T., 1987. Northward flow in the Bering and Chukchi seas. J. Geophys. Res. 92 (C7), 7097, http://dx.doi.org/10.1029/JC092iC07p07097.
Pabi, S., van Dijken, G.L., Arrigo, K.R., 2008. Primary production in the Arctic Ocean, 1998–2006. J. Geophys. Res. 113, C08005.
Palmer, M.A., Arrigo, K.R., Mundy, C.J., Ehn, J.K., Gosselin, M., Barber, D.G., Martin, J., Alou, E., Roy, S., Tremblay, J.-E., 2011. Spatial and temporal variation of photosynthetic parameters in natural phytoplankton assemblages in the Beaufort Sea, Canadian Arctic. Polar Biol. 34 (12), 1915–1928, http://dx.doi.org/10.1007/s00300-011-1050-x.
Palmer, M.A., Saenz, B.T., Arrigo, K.R., 2014. Impacts of sea ice retreat, thinning, and melt-pond proliferation on the summer phytoplankton bloom in the Chukchi Sea, Arctic Ocean. Deep-Sea Res. II 105, 85–104, http://dx.doi.org/10.1016/j.dsr2.2014.03.016.
Perovich, D.K., 1990. Theoretical estimates of light-reflection and transmission by spatially complex and temporally varying sea ice covers. J. Geophys. Res. 95, 9557–9567.
Perovich, D.K., 1998. Physics of Ice Covered Seas, 1. University of Helsinki Press, Helsinki Finland p. 446.
Perovich, D.K., Polashenski, C., 2012. Albedo evolution of seasonal Arctic sea ice. Geophys. Res. Lett. 39 (8), L08501.
Perrette, M., Yool, A., Quartly, G.D., Popova, E.E., 2011. Near-ubiquity of ice-edge blooms in the Arctic. Biogeoscience 8, 515–524.
Pickart, R.S., Pratt, L.J., Torres, D.J., Whitledge, T.E., Proshutinsky, A.Y., Aagaard, K., Agnew, T.A., Moore, G.W.K., Dail, H.J., 2010. Evolution and dynamics of the flow through Herald Canyon in the western Chukchi Sea. Deep-Sea Res., Part II 57, 5–26.
Platt, T., Gallegos, C.L., Harrison, W.G., 1980. Photoinhibition of photosynthesis in natural assemblages of marine phytoplankton. J. Mar. Res. 38, 687–701.
Polashenski, C.M., 2011. Attributing Change and Understanding Melt Ponds on a Seasonal Ice Cover (Ph.D. dissertation). Thayer School of Engineering at Dartmouth College, Hanover, New Hampshire.
Polyakov, I.V., Alekseev, G.V., Bekryaev, R.V., Bhatt, U., Colony, R.L., Johnson, M.A., Karklin, V.P., Makshtas, A.P., Walsh, D., Yulin, A.V., 2002. Observationally based assessment of polar amplification of global warming. Geophys. Res. Lett. 29 (18), 1878, http://dx.doi.org/10.1029/2001GL011111.
Reynolds, R.A., Stramski, D., Wright, V.M., Wozniak, S.B., 2010. Measurements and characterization of particle size distributions in coastal waters. J. Geophys. Res. 115, C08024.
Sakshaug, E., 1997. Biomass and productivity distributions and their variability in the Barents Sea. ICES J. Mar. Sci. 54, 341–350.
Sakshaug, E., 2004. Primary and secondary production in Arctic Seas. In: Stein, R., Macdonald, R.W. (Eds.), The Organic Carbon Cycle in the Arctic Ocean. Springer-Verlag, Berlin, pp. 57–81.
Schulze, L.M., Pickart, R.S. (2012), Seasonal variation of upwelling in the Alaskan Beaufort Sea: Impact of sea ice cover. J. Geophys. Res., 100, (in press).
Soreide, J.E., Leu, E., Berge, J., Graeve, M., Falk-Petersen, S., 2010. Timing of blooms, algal food quality and Calanus glacialis reproduction and growth in a changing Arctic. Glob. Change Biol. 16 (11), 3154–3163, http://dx.doi.org/10.1111/j.1365-2486.2010.02175.x.
Sorteberg, A., Walsh, J.E., 2008. Seasonal cyclone variability at 70°N and its impact on moisture transport into the Arctic. Tellus Ser. A 60 (3), 570–586, http://dx.doi.org/10.1111/j.1600-0870.2008.00314.x.
Sosik, H.M., Olson, R.J., 2007. Automated taxonomic classification of phytoplankton sampled with imaging in-flow cytometry. Limnol. Oceanogr. Methods 5, 204–216.
Spall, M.A., Pickart, R.S., Brugler, E.T., Moore, G.W.K., Thomas, L., Arrigo, K.R., 2014. Role of shelfbreak upwelling in the formation of a massive under-ice bloom in the Chukchi Sea. Deep-Sea Res. II 105, 17–29, http://dx.doi.org/10.1016/j.dsr2.2014.03.017.
Spilling, K., 2007. Dense sub-ice bloom of dinoflagellates in the Baltic Sea, potentially limited by high pH. J. Plank. Res. 29 (10), 895–901.
Springer, A.M., McRoy, C.P., 1993. The paradox of pelagic food webs in the northern Bering Sea—III. Patterns of primary production. Cont. Shelf Res. 13 (5-6), 575–599.
Stirling, I., 1997. The importance of polynyas, ice edges, and leads to marine mammals and birds. J. Mar. Syst. 10, 9–21.
Strass, V.H., Nothig, E.-M., 1996. Seasonal shifts in ice edge phytoplankton blooms in the Barents Sea related to the water column stability. Polar Biol. 16, 409–422.
Subba Rao, D.V., Platt, T., 1984. Primary production of Arctic waters. Polar Biol. 3, 191–201.
Sukhanova, I.N., Flint, M.V., Pautova, L.A., Stockwell, D.A., Grebmeier, J.M., Sergeeva, V.M., 2009. Phytoplankton of the western Arctic in the spring and summer of 2002: Structure and seasonal changes. Deep-Sea Res., Part II 56 (17), 1223–1236, http://dx.doi.org/10.1016/j.dsr2.2008.12.030.
Walsh, J.J., McRoy, C.P., Coachman, L.K., Goering, J.J., Nihoul, J.J., Whitledge, T.E., Blackburn, T.H., Parker, P.L., Wirick, C.D., Shuert, P.G., Grebmeier, J.M., Springer, A.M., Tripp, R.D., Hansell, D.A., Djenidi, S., Deleersnijder, E., Henriksen, K., Lund, B.A., Andersen, P., Muller-Karger, F.E., Dean, K., 1989. Carbon and nitrogen cycling within the Bering Chukchi Seas - Source regions for organic-matter effecting AOU Demands of the Arctic-Ocean. Prog. Oceanogr. 22 (4), 277–359.
Walsh, J.J., Dieterle, D.A., Maslowski, W., Grebmeier, J.M., Whitledge, T.E., Flint, M., Sukhanova, I.N., Bates, N., Cota, G.F., Stockwell, D., Moran, S.B., Hansell, D.A., McRoy, C.P., 2005. A numerical model of seasonal primary production within the Chukchi/Beaufort Seas. Deep-Sea Res., Part II 52, 3541–3576.
Wang, J., Cota, G.F., Comiso, J.C., 2005. Phytoplankton in the Beaufort and Chukchi seas: distribution, dynamics, and environmental forcing. Deep-Sea Res., Part II 52 (24-26), 3355–3368.
Wassmann, P., 2011. Arctic marine ecosystems in an era of rapid climate change. Prog. Oceanogr. 90, 1–17.
Wassmann, P., Andreassen, I., Reigstad, M., Slagstad, D., 1996. Pelagic-benthic coupling in the Nordic Seas: the role of episodic events. Mar. Ecol. 17, 447–471.
Wassmann, P., Duarte, C.M., Agusti, S., Sejr, M.K., 2010. Footprints of climate change in the Arctic marine Ecosystem. Glob. Change Biol. 17, 1235–1249.
Weingartner, T., Aagaard, K., Woodgate, R., Danielson, S., Sasaki, Y., Cavalieri, D., 2005. Circulation on the north central Chukchi Sea shelf. Deep-Sea Res., Part II 52 (24–26), 3150–3174.
Woodgate, R.A., Aagaard, K., Swift, J.H., Falkner, K.K., Smethie, W.M., 2005. Pacific ventilation of the Arctic Ocean's lower halocline by upwelling and diapycnal mixing over the continental margin. Geophys. Res. Lett. 32 (18), L18609, http://dx.doi.org/10.1029/2005GL023999.
Woodgate, R.A., Aagaard, K., 2005. Revising the Bering Strait freshwater flux into the Arctic Ocean. Geophys. Res. Let. 32 (2), L02602, http://dx.doi.org/10.1029/2004GL021747.
Woodgate, R.A., Aagaard, K., Weingartner, T.J., 2006. Interannual changes in the Bering Strait fluxes of volume, heat and freshwater between 1991 and 2004. Geophys. Res. Lett. 33, L15609.

Woodgate, R.A., Weingartner, T.J., Lindsay, R., 2012. Observed increases in Bering Strait oceanic fluxes from the Pacific to the Arctic from 2001 to 2011 and their impacts on the Arctic Ocean water column. Geophys. Res. Lett. 39 (24), L24603, http://dx.doi.org/10.1029/2012GL054092.

Yager, P.L., Connely, T.L., Mortazavi, B., Wommack, K.E., Bano, N., Bauer, J.E., Opsahl, S., Hollibaugh, J.T., 2001. Dynamic bacterial and viral response to an algal bloom at subzero temperatures. Limnol. Oceanogr. 46 (4), 790–801.

Zhang, X.D., Walsh, J.E., Zhang, J., Bhatt, U.S., Ikeda, M., 2004. Climatology and interannual variability of arctic cyclone activity: 1948–2002. J. Clim. 17 (12), 2300–2317 (10.1175/1520-0442(2004)017 < 2300:CAIVOA > 2.0.CO;2).

Zhang, J., Spitz, Y.H., Steele, M., Ashjian, C., Campbell, R., Berline, L., Matrai, P., 2010. Modeling the impact of declining sea ice on the Arctic marine planktonic ecosystem. J. Geophys. Res. 115, C10015.